Complementary Coded Multiplane Wave Sequences For SNR Increase in Ultrafast Power Doppler Ultrasound Imaging

Tamraoui Mohamed, Adeline Bernard, Roux Emannuel, Liebgott Hervé

Complementary Coded Multiplane Wave Sequences For SNR Increase in Ultrafast Power Doppler Ultrasound Imaging

Tamraoui Mohamed, *Student, IEEE*, Adeline Bernard, Roux Emannuel, and Liebgott Hervé, *Member, IEEE*

***Abstract*— Power Doppler imaging is a commonly used technique for visualizing blood flow in ultrasound imaging. This technique measures flow amplitude rather than velocity, and it relies on detecting the power of Doppler signals, making it particularly useful for detecting weak blood flow. The emergence of coherent plane wave compounding has enabled significant progress in ultrafast power Doppler imaging. However, the lack of transmit focusing leads to low Signal-to-Noise Ratio (SNR) and contrast, thereby reducing the sensitivity to blood flow, particularly in deep tissue regions. We propose to increase the SNR and contrast of ultrafast power Doppler imaging by leveraging the ideal correlation properties of Complete Complementary Codes (CCC) for Multi-Plane Wave Imaging (MPWI). The MPWI-CCC method consists of transmitting quasi-simultaneously N tilted plane waves coded with a binary sequence of length L. Subsequently, the backscattered signals from each plane wave are individually recovered with high amplitude through decoding. We compared MPWI-CCC and Multi-plane Wave Imaging with Hadamard encoding (MPWI-HD) against Coherent Plane Wave Compounding (CPWC) in both simulations and experiments. When transmitting four plane waves on a commercial blood flow phantom, MPWI-CCC exhibited SNR and contrast gains of 13.02dB and 10.08dB, respectively, compared to CPWC. MPWI-HD, on the other hand, achieved gains of only 6.99dB and 4.29dB, respectively.**

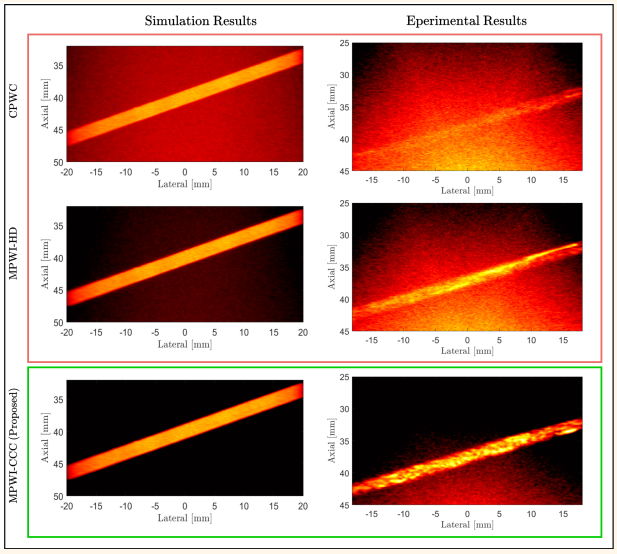

***Index Terms*— Plane wave compounding, Complete Complementary Codes, Hadamard, Multi-Plane Wave, Power Doppler, signal-to-noise ratio.**

I. Introduction

POWER Doppler ultrasound imaging involves the repeated insonification of blood vessels using ultrasonic waves. When these waves interact with a blood vessel, a portion of their energy is reflected back by red blood cells and subsequently detected by the probe in the form of radiofrequency (RF) signals. Following the necessary processing and beamforming steps, the RF signals are used to extract the mean intensity of the Doppler signal at each pixel, ultimately producing a power Doppler image. While power Doppler does not provide information about blood velocity, it is a valuable tool thanks to its association with the volume of blood within a given pixel [1], [2]. This characteristic makes it a useful tool in various applications including micro-vascularization imaging [3], [4] and mapping of brain activity in functional ultrasound imaging [5]–[7].

Conventional ultrasound imaging relies on the transmission of focused ultrasound beams. During each transmission, the recorded RF signals are beamformed to reconstruct a single image line. The entire image is generated by scanning the imaging area sequentially, line by line. This sequential approach can limit the frame rate, potentially leading to aliasing in Doppler images [6]. To mitigate aliasing in conventional Doppler imaging, the image is divided into blocks with a limited number of lines, and each block is scanned only a few times at a high frame rate [8]. However, this strategy imposes restrictions on the number of acquired spatial and temporal samples, which, in turn, reduces the Doppler sensitivity, particularly for small vessels with low blood flow [6], [9].

This work was supported by the LABEX PRIMES under Grant ANR-11-LABX-0063 of Université de Lyon, through the Program “Investissements d’Avenir” under Grant ANR-11-IDEX-0007 operated by the French National Research Agency (ANR), performed within the framework of the ANR-20-CE19-0023 SPARTECHUS. This material is based upon work done on the PILoT facility (PILoT, INSA-Lyon).

The authors are with the Univ Lyon, INSA-Lyon, Université Lyon 1, CNRS, Inserm, CREATIS UMR, France.

Highlights

- **This study introduces MPWI-CCC, a new multi-plane wave imaging technique based on complete complementary codes to increase the SNR and sensitivity of ultrafast power Doppler Imaging.**
- **MPWI-CCC was experimentally validated, yielding power Doppler images with strong blood flow signals and achieving SNR and contrast gains of 13.02dB and 10.08dB, respectively compared to CPWC, when transmitting with 4 plane waves.**
- **MPWI-CCC will improve the detection of small blood vessels with weak blood flow, particularly in deep regions or in patients with thick abdominal walls or tissue where bones might be present.**

The emergence of high frame rate ultrasound has enabled significant progress in blood flow quantification. Instead of the traditional line-by-line transmission method, ultrafast imaging relies on the use of spherical waves in synthetic transmit aperture imaging [10], [11] or plane waves in plane wave imaging [12], [13]. This approach enables the simultaneous acquisition of data of the entire image, effectively decoupling the number of transmissions from the image size and resulting in high imaging frame rates. Although both synthetic aperture imaging and plane wave imaging have demonstrated significant improvements in blood flow imaging, plane wave imaging is the most widely used technique for blood flow applications in the literature. When the technique was first introduced in [12], a single Plane Wave (PW) transmission was used to insonify the entire field of view, and the resulting backscattered echoes were reconstructed into an image. With only one transmission required, ultrafast imaging achieves frame rates of several thousand frames per second, depending on the imaging depth. However, because no transmit focusing occurs, the image quality is considerably compromised, particularly in terms of spatial resolution and contrast, when compared to conventional focused imaging. Coherent Plane Wave Compounding (CPWC) was introduced to enhance the image quality of ultrafast plane wave imaging [14], [15]. Instead of transmitting a single plane wave, this technique involves sequentially transmitting several titled plane waves at varying angles. The resulting beamformed images for each angle are then coherently compounded to reconstruct high-quality images.

It has been reported that, thanks to its high frame rate, ultrafast Doppler imaging using CPWC, has significantly enhanced power Doppler sensitivity, with an increase by a factor of up to 30 when compared to conventional Doppler imaging [6]. This improvement is primarily due to the fact that all the image pixels are acquired simultaneously within a short period of time with a large temporal ensemble [9]. This has ensured very high temporal correlation between frames which allows the use of a singular value decomposition (SVD) clutter filter which has proven to be very effective in discerning relatively slow blood flow in small vessels from tissue motion [16], [17]. Nevertheless, CPWC introduces a trade-off between frame rate and image quality [14], [18]. Essentially, as the number of transmitted angles increases, the image quality improves. However, concurrently, this increase in image quality comes at the cost of a reduction in frame rate and the effective pulse repetition frequency (PRF) in flow imaging application which reduces the maximum flow velocity that can be estimated [19].

To maintain a high frame rate, it is preferable to transmit a small number of plane waves, an approach that, however, comes at the cost of reducing the signal-to-noise ratio (SNR) [14], [20], [21]. Moreover, patients with thick abdominal walls or the presence of bone in the tissue, such as the skull, results in significant attenuation of acoustic waves, further diminishing the SNR [20], [22], [23]. This reduction in SNR decreases the sensitivity to the blood flow in small and deep vessels. The injection of contrast agent can enhance the backscattering signals thus improving the SNR [24], [25]. However, this procedure is invasive and complex. Additionally, when contrast agents are used, the transmit pressure needs to be kept at a low level to avoid destroying the microbubbles and thus increasing their life time [26]. This is often achieved by reducing the transmit voltage (typically to around 5 to 10 volts), which in turn reduces the overall SNR. An alternative approach that can increase the SNR without using contrast agent is coded excitation [27].

The SNR is directly proportional to the transmitted energy. Coded excitation consists in increasing the transmitted energy without compromising axial resolution nor the FDA safety limits [28]. This technique has been proven to substantially enhance ultrasound imaging capabilities by spatially encoding the transmitted plane waves or using long modulated signals.

In the spatial encoding category, a Multiplane Wave Imaging method using Hadamard encoding (MPWI-HD) has been proposed to enhance the SNR of ultrafast images without reducing the frame rate [20]. In this technique, multiple tilted plane waves are quasi-simultaneously transmitted using short pulses encoded by a Hadamard matrix. In reception, decoding is carried out using the inverse of the Hadamard matrix. The signals from each tilted PW are decoded through simple addition and subtraction operations, resulting in an SNR increase of $10\log_{10}(N)$ compared to CPWC, where N represents the number of PW. MPWI-HD has been applied to ultrafast power Doppler imaging of the rat brain through the skull [29]. It has demonstrated enhanced sensitivity in Doppler imaging, enabling the detection of deeper blood vessels within the brain. Nevertheless, it is worth to note that improving the SNR with MPWI-HD remains tied to the number of transmitted plane waves. Moreover, due to the properties of Hadamard matrices, the number of transmitted plane waves is even and confined to a power of 2. Similarly, to MPWI-HD, Cascaded Dual-polarity Waves Imaging (CDWI) was introduced by designing a novel encoding matrix [30], [31]. In contrast to the square Hadamard matrix, this encoding matrix have a size of $M \times N$, where M is an even number (number of transmissions), and N equals 2^k (number of tilted plane waves), with k being an integer. In each of the M transmissions, N cascaded dual-polarity waves

are transmitted. The decoding process involves applying delays to realign the waves and performing addition and subtraction operations, similarly to MPWI, resulting in an SNR gain of $10\log_{10}(N)$. However, since decoding is done after several emissions, tissue motion and the nonlinear propagation of ultrasonic waves in the tissue result in imperfect cancellation of negative and positive pulses after decoding, leading to the appearance of range side-lobes artifacts [30], [32].

Coded excitation techniques involving long modulated excitation signals have also been investigated to increase the transmitted energy while respecting the FDA safety limits [33]. These methods involve a decoding step using pulse compression to restore axial resolution while increasing the SNR. In [4], a linear frequency modulated chirp was used to enhance the sensitivity of an ultrasound arthroscopic probe used for imaging meniscus vascularization during surgery. In this approach, a chirp was used as an excitation signal for CPWC combined with a mismatched filter for pulse compression to reduce axial side-lobes. Although high SNR gains in power Doppler images were achieved compared to conventional CPWC and MPWI, the mismatch filtering operation does not completely suppress axial side-lobes and comes at the cost of reducing axial resolution. In [23], a phase modulation sequence based on a compound Barker code was introduced to enhance sensitivity in Transcranial power Doppler imaging. Barker codes are known for their low axial side-lobes. To suppress axial side lobes, decoding was performed using an inverse filtering approach [34]. However, while axial side lobes can be suppressed, this approach reduces SNR gains. Moreover, only 7 barker codes exist with lengths ranging from 2 to 13 bits which can restrict their use in applications requiring diverse sequences. While compound Barker codes extend the code length while maintaining their frequency domain properties, they increase sidelobe levels, leading to potential artifacts if only matched filtering is used instead of inverse filtering.

Although the previous cited methods have shown promise in enhancing ultrasound imaging capabilities, they also exhibit notable limitations. One of these limitations is the challenge to increase the SNR and sensitivity of ultrasound power Doppler imaging without increasing the number of transmissions or introducing sidelobe artifacts in the images. In this context, our study introduces a novel approach designed to address these shortcomings. In this work, we propose a new coded excitation scheme for ultrafast plane wave imaging to increase the sensitivity of power Doppler imaging. This approach is based on the Multi-Plane Wave Imaging method (MPWI) [20], but instead of spatial encoding using a Hadamard matrix, a phase modulated sequence will be used. Here we propose the use of Complete Complementary Codes (CCC) [35] that we have recently introduced to increase the SNR in 3D synthetic transmit aperture with a sparse 2D array [36]. These codes, often denoted as (M, N, L)-CCC, consist of M sets, each having N binary sequences of length L bits. CCC are known for their ideal auto-correlation (i.e., delta impulse) and ideal cross-correlation function (i.e., zero at all shifts) which makes them ideal for simultaneous sequence transmission. Consequently, during decoding, no axial sidelobes are introduced, eliminating the need for mismatch filtering or inverse filtering. Thus, ultrafast power Doppler imaging using Multi-Plane Wave Imaging with Complete Complementary Codes (MPWI-CCC) benefits from the quasi-simultaneous transmission of plane waves of MPWI and from the ideal correlation properties of CCC to decode the received signals. Unlike the methods suggested in [4], [23], which involves transmitting a single plane wave using a modulated signal during each transmission, MPWI-CCC allows for the quasi-simultaneous transmission of multiple tilted plane waves, each transmitting a different phase modulated signal. By transmitting CCC sequences, the proposed method offers the possibility to increase the SNR by increasing the length of the sequence without increasing the number of transmissions. An SNR gain of $10\log_{10}(NL)$ compared to CPWC is obtained. This results in increased sensitivity to blood vessels, especially small ones with weak blood flow, particularly in deep regions or tissues where bones might be present, such as the skull.

II. MATERIAL AND METHODS

A. Complete Complementary Codes (CCC)

The CCC are composed of M sets of N binary sequences. Consider the following $M \times N$ matrix of binary sequences:

$$\mathcal{C} = \begin{bmatrix} S_1 \\ S_2 \\ . \\ S_M \end{bmatrix} = \begin{bmatrix} \boldsymbol{s}_{1,1} & \boldsymbol{s}_{1,2} & ... & \boldsymbol{s}_{1,N} \\ \boldsymbol{s}_{2,1} & \boldsymbol{s}_{2,2} & ... & \boldsymbol{s}_{2,N} \\ . & . & ... & . \\ \boldsymbol{s}_{M,1} & \boldsymbol{s}_{M,2} & ... & \boldsymbol{s}_{M,N} \end{bmatrix} \tag{1}$$

Each row corresponds to the m^{th} set of N binary sequences (± 1) $s_{m,n}$ of length L. We call $\mathcal{C}$ an (M, N, L)-$Sequence\ Family$. The (M, N, L)-$Sequence\ Family$ becomes a (M, N, L)-CCC if the sum of the auto-correlation functions (ACF) in each set S_m is zero except for the zero shift (i.e., delta impulse), and if for any pair of different sets, the sum of the cross-correlation functions (CCF) between sequences at the same index is zero at all shifts. In other words, a $(M, N, L) - CCC$ verifies the following :

$$\sum_{j=1}^{N} R_{s_{m,j}}(\tau) = ML\delta(\tau) \tag{2}$$

$$\sum_{j=1}^{N} R_{s_{m,j},s_{n,j}}(\tau) = 0 \tag{3}$$

where $m \neq n \in (1, 2, ..., M)$. $R_{s_{m,j}}(\tau)$ is the ACF of sequence $s_{m,j}$ and $R_{s_{m,j},s_{n,j}}(\tau)$ is the CCF between the sequences $s_{m,j}$ and $s_{n,j}$. ML corresponds to the energy of the delta function.

Various methods to create CCC sets employing different set sizes (N) and sequence lengths (L), have been proposed in the literature. In this context, we adopt the method introduced in [35] to generate an $(N, N, MN/P)$-CCC with $(M, N, P \in Z^+; M, P \leq N)$ and the condition that P should divide into N, and M divide into N/P. This approach enables the generation of N sets, containing each N sequences. The interesting feature of this method lies in the capability of controlling the length $L = MN/P$ (power of 2) of the

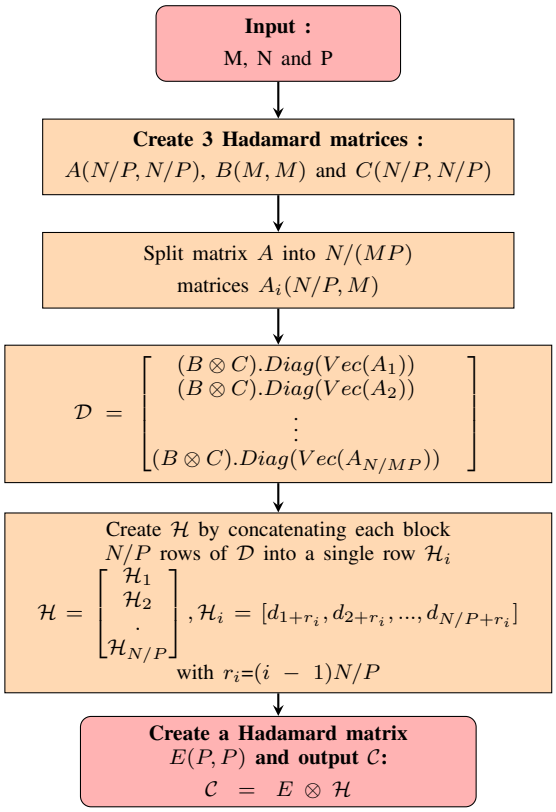

Fig. 1: Flowchart of the $(N, N, MN/P)$-CCC generation process.

binary sequences with the maximum length possible being ($L = N^2$). By selecting different values for M and P, the method allows the generation of either short or long sequences, depending on the user's needs. Fig. 1 shows a flowchart of the $(N, N, MN/P)$-CCC generation process. For more details on the construction method, refer to [35], [36].

An example of $(N, N, MN/P)$-CCC is given bellow, with $M = 2$, $N = 4$, $P = 2$ which corresponds to $(4, 4, 4)$-CCC :

$$\begin{aligned}
&\boldsymbol{s}_{1,1} = (++-+) \quad \boldsymbol{s}_{1,2} = (+---) \quad \boldsymbol{s}_{1,3} = (++-+) \quad \boldsymbol{s}_{1,4} = (+---)\\
&\boldsymbol{s}_{2,1} = (+++-) \quad \boldsymbol{s}_{2,2} = (+--++) \quad \boldsymbol{s}_{2,3} = (+++-) \quad \boldsymbol{s}_{2,4} = (+--++)\\
&\boldsymbol{s}_{3,1} = (++-+) \quad \boldsymbol{s}_{3,2} = (+---) \quad \boldsymbol{s}_{3,3} = (---+) \quad \boldsymbol{s}_{3,4} = (-++-)\\
&\boldsymbol{s}_{4,1} = (+++-) \quad \boldsymbol{s}_{4,2} = (+--++) \quad \boldsymbol{s}_{4,3} = (---+) \quad \boldsymbol{s}_{4,4} = (-++-)
\end{aligned}$$

Where $+$ denotes $+1$ and $-$ denotes -1. The MATLAB code used to generate the binary sequences and reproduce the experiments in this paper is publicly available in a GitHub repository: https://github.com/Tamraoui/CompleteComplementaryCodes.

B. Multiplane Wave Imaging using Hadamard Encoding (MPWI-HD)

MPWI-HD [20] enables an increase of the transmitted signal amplitude without the necessity of increasing the number of transmissions. It involves the quasi-simultaneous transmission of multiple tilted plane waves, with an encoding from the Hadamard matrix. Consider the case of two transmissions of two plane waves with tilted angles α_1 and α_2:

$$\begin{aligned}
x_1 &= a_{1,1}.e_{\alpha_1}(t) + a_{1,2}.e_{\alpha_2}(t) * \delta(t-\tau)\\
x_2 &= a_{2,1}.e_{\alpha_2}(t) + a_{2,2}.e_{\alpha_2}(t) * \delta(t-\tau)
\end{aligned} \tag{4}$$

During the first transmission event, two plane waves with tilted angles α_1 and α_2 are quasi-simultaneously transmitted by the probe excited by a short pulse $e(t)$ for each plane wave, separated by a very small time delay represented by τ. Each of these plane waves is multiplied by a coefficient, denoted as $a_{1,1}$ and $a_{1,2}$ respectively. During the second transmission event, the same plane waves are transmitted, but with different coefficients $a_{2,1}$ and $a_{2,2}$. These multiplicative coefficients are derived from a Hadamard matrix of order N, where N is the number of plane waves (equivalently, transmissions). In the specific case of two plane waves, a Hadamard matrix of order two is used, and it is given by:

$$H = \begin{bmatrix} a_{1,1} & a_{1,2} \\ a_{2,1} & a_{2,2} \end{bmatrix} = \begin{bmatrix} +1 & +1 \\ +1 & -1 \end{bmatrix} \tag{5}$$

The received backscattered signals after each transmission event are expressed as:

$$\begin{aligned}
y_1 &= e_{\alpha_1}(t) * h(t) + e_{\alpha_2}(t) * \delta(t-\tau) * h(t)\\
y_2 &= e_{\alpha_2}(t) * h(t) - e_{\alpha_2}(t) * \delta(t-\tau) * h(t)
\end{aligned} \tag{6}$$

Where $h(t)$ represents the impulse response of the probe and the medium. To separate the contribution of each plane wave and retrieve the echoes with higher SNR, a decoding step is necessary. This is accomplished through the following addition and subtraction operations :

$$\begin{aligned}
y_{\alpha_1} &= y_1 + y_2 = 2.e_{\alpha_1}(t) * h(t)\\
y_{\alpha_2} &= y_1 - y_2 = 2.e_{\alpha_2}(t) * \delta(t-\tau) * h(t)
\end{aligned} \tag{7}$$

The addition operation allows the signal suppression of the plane wave with angle α_2, leaving only signals from the plane wave with angle α_1 with an amplitude twice higher than simple transmission of one plane wave at a time (CPWC). Conversely, the subtraction operation suppresses the contribution of the plane wave with angle α_1 and doubles the amplitude of the signals of the plane wave with angle α_2. In this case, a gain in SNR of $10\log_{10}(2) = 3.01$dB is achieved compared to CPWC. When generalizing MPWI-HD to N plane waves with N transmissions, the method yields a theoretical gain of $10\log_{10}(N)$. However, N is restricted to a power of 2 as the coding is directly linked to the size of the Hadamard matrix.

C. Multi-Plane Wave Imaging with Complete Complementary Codes (MPWI-CCC)

While MPWI-HD can enhance the SNR of the recovered RF signals, it is important to note that the improvement is constrained by the order of the matrix. With MPWI-CCC, we free this constraint by replacing the Hadamard matrix by the CCC to create the binary sequences that will be transmitted. For MPWI-CCC, $(N, N, MN/P)$-CCC binary sequences are used for quasi-simultaneous plane waves transmission, where N corresponds to the number of angles (equivalently, transmissions). Each set of the $(N, N, MN/P)$-CCC is then assigned to a tilted plane wave. During each transmission, N tilted

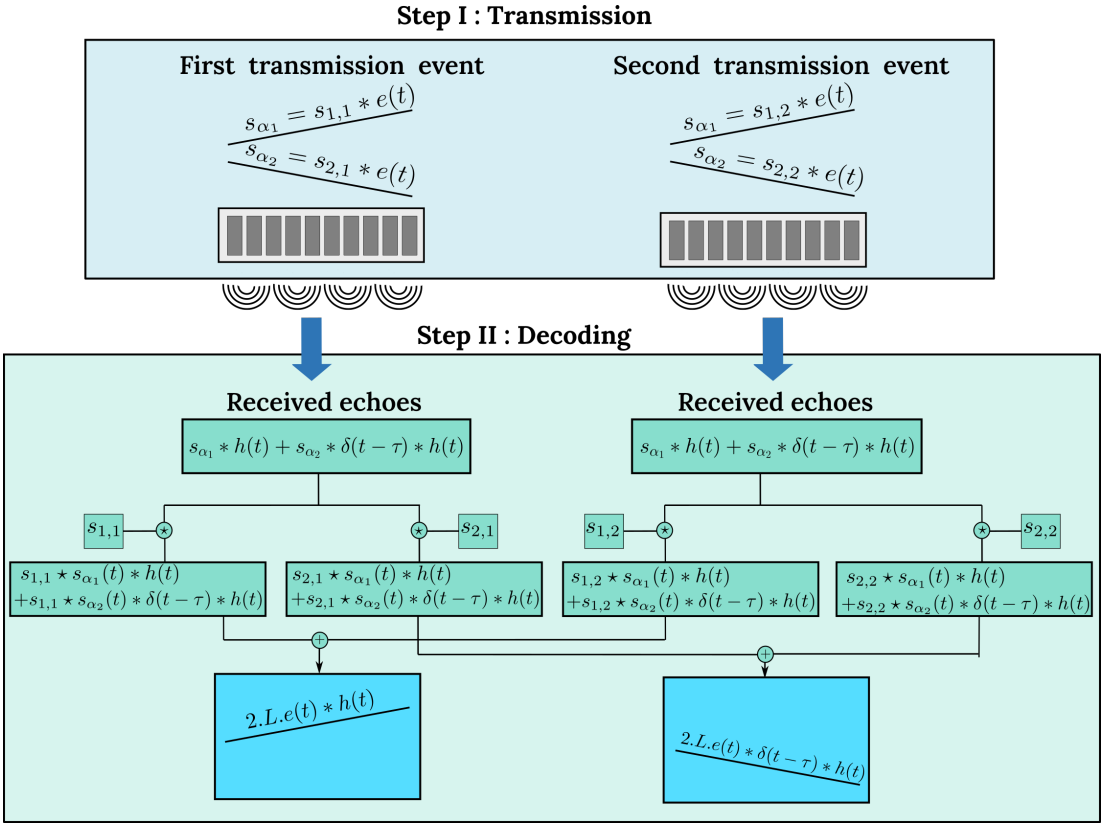

Fig. 2: Overview of MPWI-CCC imaging transmission and decoding scheme using $(\mathrm{N}, \mathrm{N}, \mathrm{MN/P})$-CCC.

angles are quasi-simultaneously transmitted with a short time delay τ. Each tilted angle transmits a different sequence from the corresponding $(N, N, MN/P)$-CCC set assigned to it.

In practice, the binary $(N, N, MN/P)$-CCC sequences are not transmitted directly by the transducer because the spectrum of a binary code contains high harmonics that cannot be easily transmitted and received by the transducer. Instead of directly transmitting the binary sequences, they are used to modulate a base pulse $e(t)$ by oversampling the sequence and convolving it with the base pulse. $e(t)$ is usually a sinewave at the central frequency of the transducer with a phase of 0° for a +1 bit and a phase of 180° for a -1 bit. This modulation makes good use of the transducer bandwidth and maximizes the transmitted energy [27], [37].

Following N transmissions, and leveraging the ideal auto-correlation and cross-correlation properties CCC, the received signals are decoded without any interference between plane waves assuming a linear propagating medium without considering motion. This decoding process allows the separation of the contribution of each plane wave. Consequently, the ultrafast plane wave data set is recovered as if a single plane wave was transmitted during each transmission event, but with a significantly higher SNR. Under the assumption of an ideal linear propagating medium, the gain in SNR would be $10\log_{10}(NL)$, where L is the number of bits in the sequences (equal to MN/P in the case of $(N, N, MN/P)$-CCC).

To illustrate the principal of MPWI-CCC, we detail the example of two transmissions (N=2) with two tilted plane waves α_1 and α_2 represented in Fig. 2. In this case $(2, 2, MN/P)$-CCC are generated using the algorithm described in Fig. 1 :

$$\mathcal{C} = \begin{bmatrix} s_{1,1} & s_{1,2} \\ s_{2,1} & s_{2,2} \end{bmatrix} \tag{8}$$

Sequences $s_{1,1}$ and $s_{1,2}$ are assigned to the plane wave tilted with angles α_1 while sequences $s_{2,1}$ and $s_{2,2}$ are assigned to the plane wave tilted with angles α_2. During the first transmission event, the two plane waves are quasi-simultaneously transmitted by the probe, separated by a very small time delay τ that corresponds to the time required to transmit one bit to avoid overlap. The plane wave α_1 transmits the sequence $s_{1,1}$ convoluted with the base pulse $e(t)$ and the plane wave α_2 transmit the sequence $s_{2,1}$ convoluted with the base pulse $e(t)$. During the second transmission event, the plane wave α_1 transmits the sequence $s_{1,2}$ convoluted with the base pulse $e(t)$ and the plane wave α_2 transmit the sequence $s_{2,2}$ convoluted with the base pulse $e(t)$. This can be expressed as follows :

$$\begin{aligned} x_1 &= s_{1,1} * e_{\alpha_1}(t) + s_{2,1} * e_{\alpha_2}(t) * \delta(t-\tau) \\ x_2 &= s_{1,2} * e_{\alpha_1}(t) + s_{2,2} * e_{\alpha_2}(t) * \delta(t-\tau) \end{aligned} \tag{9}$$

The received backscattered signals after each transmission event are expressed as:

$$\begin{aligned} y_1 &= s_{1,1} * e_{\alpha_1}(t) * h(t) + s_{2,1} * e_{\alpha_2}(t) * \delta(t-\tau) * h(t) \\ y_2 &= s_{1,2} * e_{\alpha_1}(t) * h(t) + s_{2,2} * e_{\alpha_2}(t) * \delta(t-\tau) * h(t) \end{aligned} \tag{10}$$

Where $h(t)$ still represents the impulse response of the probe and the medium.

To separate the contribution of each tilted plane wave, the decoding operation leverages the ideal correlation properties of CCC. Following each transmission, the received signals are correlated with the sequences transmitted by each plane wave during that event. In this case, after the first transmission event, the received signals y_1 are correlated with the sequences $s_{1,1}$ and $s_{2,1}$, and after the second transmission event, the recieved signals y_2 correlated with sequences $s_{1,2}$ and $s_{2,2}$:

$$\begin{aligned} y_1^{\alpha_1} &= s_{1,1} \star s_{1,1} * e_{\alpha_1}(t) * h(t) + s_{1,1} \star s_{2,1} * e_{\alpha_2}(t) * \delta(t-\tau) * h(t) \\ y_1^{\alpha_2} &= s_{2,1} \star s_{1,1} * e_{\alpha_2}(t) * h(t) + s_{2,1} \star s_{2,1} * e_{\alpha_2}(t) * \delta(t-\tau) * h(t) \\ y_2^{\alpha_1} &= s_{1,2} \star s_{1,2} * e_{\alpha_1}(t) * h(t) + s_{1,2} \star s_{2,2} * e_{\alpha_2}(t) * \delta(t-\tau) * h(t) \\ y_2^{\alpha_2} &= s_{2,2} \star s_{1,2} * e_{\alpha_2}(t) * h(t) + s_{2,2} \star s_{2,2} * e_{\alpha_2}(t) * \delta(t-\tau) * h(t) \end{aligned} \tag{11}$$

Given that the sum of ACF of each CCC set is a delta function, and the sum of CCF between sequences at the same index in each different set is zero, summing $y_1^{\alpha_1}$ and $y_2^{\alpha_1}$ suppresses the contribution of α_2 angle, keeping only signals from α_1 plane wave with a higher amplitude. Similarly, the addition of $y_1^{\alpha_2}$ and $y_2^{\alpha_2}$ suppresses the contribution of the α_1 plane wave, preserving only the contribution of α_2 plane wave with a higher amplitude. The gain in amplitude in this case is equal to $2.L$ with L being the length if the sequences. By setting $M = 2$ and $P = 1$ sequence of 4 bits can be generated leading to an SNR gain of $10\log_{10}(N.L) = 10\log_{10}(8) = 9\text{dB}$ which is higher than the gain that can be obtained with MPWI-HD.

D. Simulation Study

In order to evaluate the performance of the proposed MPWC-CCC compared to CPWC and MPWI-HD in an ideal and fully controlled setup, Field II [38], [39] simulations have been performed including a tissue-mimicking phantom and a flow phantom. The compared imaging sequences were simulated using a 128-element linear array (pitch 0.3 mm) with a central frequency of 5 MHz, a sampling frequency of 100 MHz and a -6dB fractional bandwidth of 60% for each transducer element. Plane wave imaging was conducted using 2 plane waves (-1°, 1°), 4 plane waves (-3°, -1°, 1°, 3°), and 8 plane waves (-7°, -5°, -3°, -1°, 1°, 3°, 5°, 7°). Both CPWC and MPWI-HD were simulated using a 1-cycle Hanning-weighted sine wave at the central frequency of the transducer. For MPWI-CCC, by setting M=2, (2, 2, 4)-CCC with P=1 was used for 2 angles transmission, (4, 4, 4)-CCC with P=2 was used for 4 angles transmission, and (8, 8, 4)-CCC with P=4 was used for 8 angles transmission. All the CCC sequences were used to modulate the same short pulse used for CPWI and MPWI-HD. To simulate noisy conditions, additive white gaussian noise was generated with respect to the bandwidth of the transducer using a pass-band filter. The noise was first generated for CPWI and the same noise energy was added to the RF data of MPWI-HD and MPWI-CCC before decoding. Frequency-dependent attenuation was excluded in simulations to assess the imaging schemes in ideal propagation conditions and verify theoretically expected SNR gains.

1) Tissue Phantom simulation: To evaluate the performance of the three imaging schemes in B-mode imaging and assess the sidelobe levels introduced by the encoding methods (MPWI-HD and MPWI-CCC), isolated Point Spread Functions (PSFs) were simulated. Both stationary PSFs and axially moving PSFs, using the same speed and PRF as in the flow experiments, were simulated to assess the effect of motion on the decoding performance of MPWI-HD and MPWI-CCC. Additionally, a tissue-mimicking phantom was simulated under 5dB SNR conditions. The phantom, measuring $40 \times 40\text{mm}^2$, consists of randomly distributed scatterers with a reflection coefficient following a normal Gaussian distribution and a density of 10 scatterers per resolution cell. Within the phantom, an anechoic inclusion (Cyst) with a diameter of 8 mm was positioned at a depth of 60 mm. Additionally, the phantom included 5 wires with a diameter equal to 1 wavelength by clustering several point scatterers within a circular region corresponding to the desired diameter. All scatterers were assigned the same amplitude to mimic a uniform scattering response across the wire.

2) Flow Phantom simulation: To assess the performance of the three imaging schemes in blood flow imaging a tissue phantom containing a small blood vessel was simulated. The blood vessel, with a radius of 2 mm, was positioned at 40 mm depth from the center of the probe, and it had a beam-to-flow angle of 18°. The number of tissue and blood scatterers was 10 per resolution cell with tissue scatterers having a reflection coefficients amplitude 30dB higher than blood scatterers. The scatterers in the blood vessel were moved between emissions with a maximum flow rate of 2ml/s. To achieve an imaging frame rate of 800 Hz The pulse repetition frequency (PRF) of plane wave imaging was adjusted based on the number of plane waves. For each imaging scheme, an ensemble of 200 frames was simulated under -10dB SNR conditions relative to the blood signal.

E. Experimental Study

The performance of MPWC-CCC was also experimentally evaluated using an ultrasound imaging research platform (Verasonics Inc., Redmond, WA) equipped with the Philips ATL L7-4 linear array transducer (128 elements, pitch 0.3 mm). The transducer had a central frequency of 5 MHz, a fractional bandwidth of 60%, and operated at a sampling frequency of 20 MHz. The same plane wave imaging setup that was used for simulation, for the three imaging schemes, was also used during the experimental acquisition for 2, 4 and 8 plane waves. For MPWI-CCC, the Arbitrary Waveform Generation Toolbox (ArbWave Toolbox in Verasonics), provided by the Vantage scanner, was employed to convert the $(N, N, MN/P)$-CCC signals generated following the procedure described in Fig. 1 into tristate signals that can be transmitted by the scanner.

Measurements were conducted on a wire phantom in water to mimic a PSF in order to assess if the encoding methods give rise to axial sidelobes and show the actual influence of the imaging system. Then, flow experiments were performed using a commercial Doppler flow phantom setup, comprising a Doppler flow pump (Model: 769, CIRS) and the Doppler flow phantom (Model: ATS 523A, CIRS). This configuration emulated blood flow in a tissue-mimicking phantom. A Doppler fluid, with a continuous slow rate of 0.2 ml/sec, was pumped

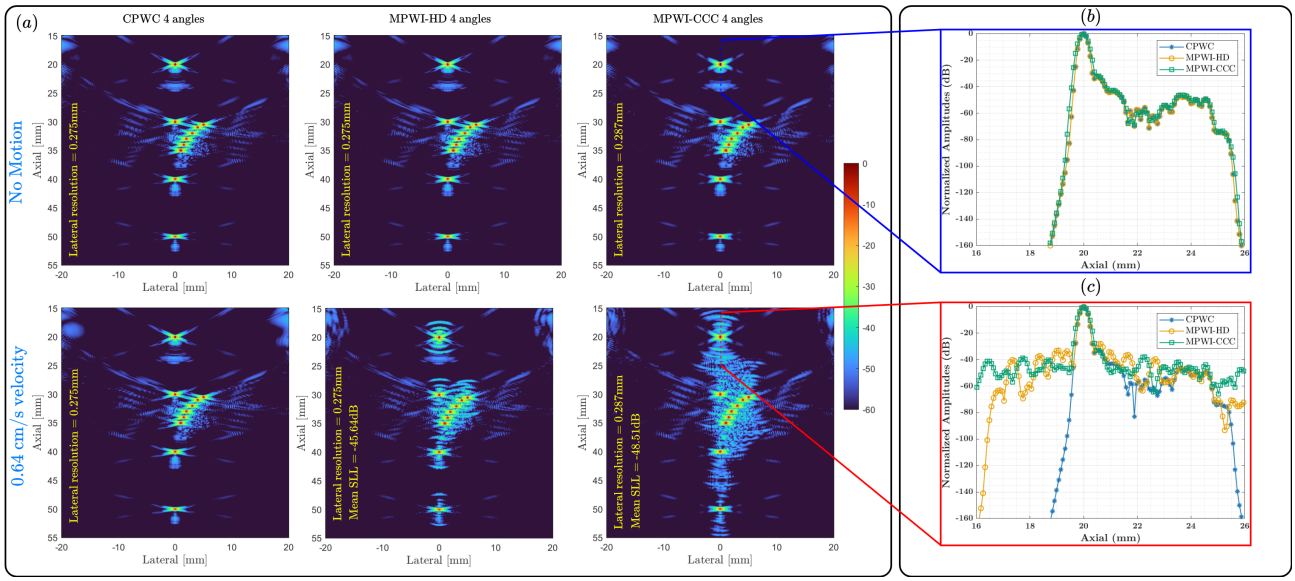

Fig. 3: The simulated B-mode images of isolated PSFs for CPWC, MPWI-HD and MPWI-CCC for 4 plane waves transmissions in the absence and the presence of motion. (B) Axial line plot highlighting the level sidelobes introduced by MPWI-HD and MPWI-CCC.

through a 2 mm flow channel angled at 18°. The PRFs used in the experiments where adjusted to achieve an imaging frame rate of 800 Hz based on the number of transmitted plane waves. PRFs of 1600 Hz, 3200 Hz, and 6400 Hz were used for 2, 4, and 8 plane wave transmissions, respectively.

F. Image Quality Metrics

The performance of the emission schemes was evaluated for B-mode imaging and power Doppler imaging. For B-mode imaging, the Peak Signal-to-Noise Ratio (PSNR), Contrast Ratio (CR) and the axial resolution were computed. The PSNR was calculated on the 5 scatterers positioned to the right of the tissue-mimicking phantom using the following formula:

$$(\mathrm{PSNR})_{dB} = 20\log_{10}\left(\frac{\max(S_{scat})}{\sigma_{noise}}\right) \tag{12}$$

Where $\max(S_{scat})$ is the peak signal of the scatterer and σ_{noise} is the root mean square of the noise inside the anechoic inclusion. Additionally, the CR was computed on the same images as follows :

$$(\mathrm{CR})_{dB} = 20\log_{10}\left(\frac{\mu_{cyst}}{\mu_{bck}}\right) \tag{13}$$

Where μ_{cyst} and μ_{bck} are the mean image intensities respectively inside the anechoic inclusion and in the surrounding background. The axial and lateral resolutions at $-6\mathrm{dB}$ was computed on the single scatterer on the left of the phantom. Additionally, the sidelobes level was assessed by calculating the mean sidelobes level for values above -60 dB in the region surrounding the main lobe.

For power Doppler imaging, to assess the strength of the blood flow signal, the Signal-to-Noise Ratio (SNR) was computed as a measure of the blood flow signal power relative to the power of noise, as follows:

$$(\mathrm{SNR})_{dB} = 20\log_{10}\left(\frac{\sqrt{\frac{1}{N}\sum_{i=1}^{N} I_b(i)^2}}{\sqrt{\frac{1}{N}\sum_{i=1}^{N} I_n(i)^2}}\right) \tag{14}$$

Where I_b and I_n represent the intensities of pixels of blood and noise, respectively, inside and outside blood flow (with the same number of pixels N) as illustrated on Fig 6. To measure the detectability of blood flow the CR has been computed on power Doppler images using the formula in (13) where μ_{cyst} and μ_{bck} represent in this case the mean image intensities respectively inside and outside blood flow and in the same regions used to compute the SNR.

III. Results

A. Simulation Results

The simulated B-mode images of the PSFs obtained with four plane wave transmissions are shown in Fig. 3(a) for CPWC, MPWI-HD, and MPWI-CCC. A visual inspection indicates that, in the absence of motion, both encoding methods do not introduce additional axial sidelobes after decoding, and the resulting images are similar to those obtained with CPWC. No noise was added during the simulation to avoid masking potential sidelobes. This observation was confirmed by plotting an axial line across the scatterer at a depth of 20 mm for the three methods, as shown in Fig. 3(b). The only sidelobes present are those induced by ghost sidelobes in front of the scatterers in plane wave imaging, as explained in [40].

In the presence of motion, both MPWI-HD and MPWI-CCC generate axial sidelobes with different spatial extents and magnitudes. From both Fig. 3(a) and Fig. 3(c), it can be seen that MPWI-HD exhibits higher sidelobe peaks around the scatterer mainlobe, while their magnitude gradually decreases away from it, resulting in a mean sidelobes level of -45.64 dB. On the other hand, the sidelobes obtained with MPWI-CCC have lower peaks around the main lobe and lower

overall magnitude compared to MPWI-HD, but they do not decrease in magnitude away from the scatterer, yielding a mean sidelobes level of -48.51 dB. Although both methods introduce sidelobes in the presence of motion, they remain within an acceptable level and can be further reduced using motion compensation techniques or by increasing the PRF, as discussed in section IV. Aditionally, these motion artifacts did not affect the lateral resolution as reported in Fig. 3.

The simulated B-mode images of the tissue-mimicking phantom obtained with 2 and 4 plane waves are depicted in Fig. 4. In all imaging schemes (CPWC, MPWI-HD and MPWI-CCC), the images were simulated under a +5dB noise condition and beamformed using the Delay-and-Sum (DAS) [41]–[43]. The images obtained with 2 plane waves and 4 plane waves are presented with a dynamic range of -60dB. A qualitative visual comparison of the presented results show that both MPWI-HD and MPWI-CCC enhance the SNR whatever the number of PWs that were transmitted (2 or 4 plane waves). In fact, the anechoic inclusion in the images produced by CPWC is challenging to distinguish from the surrounding tissue due to the presence of noise. On the contrary, it becomes more visible in the images produced by the two coded excitation schemes. Although both MPWI-HD and MPWI-CCC improve image quality, the visual assessment indicates that the proposed MPWI-CCC scheme produces images of superior quality compared to MPWI-HD. The next paragraph will explore quantitative analysis to confirm this observation.

The visual assessment is corroborated by computing the PSNR for the 5 scatterers at azimuth 10 mm (green box in Fig. 4) for each imaging scheme as depicted in Fig. 6(a) for the 4 plane waves transmissions case. In comparison to CPWC, MPWI-HD exhibits an average SNR gain of 6.51dB, while the proposed MPWI-CCC achieves a average SNR gain of 12.98dB. In Fig. 6(b), the SNR gains obtained with MPWI-HD and MPWI-CCC compared to CPWC are shown. These values are computed by the difference in the SNR, as calculated using Equation 12 for Fig. 6(a), for MPWI-HD and CPWC, as well as MPWI-CCC and CPWC. The values are then averaged over the 5 scatterers in the case of 2, 4, and 8 plane waves to determine the SNR gain obtained with each method. Conversely, MPWI-CCC demonstrates superior SNR gains with 8.42dB and 15.2dB, respectively. Considering an ideal, linear propagation medium in the simulations, a constant SNR gain is obtained as a function of depth. In an additional experiment, MPWI-CCC simulations were conducted using different (N, N, MN/P)-CCC sequence lengths to assess the impact of increasing the number of bits on the SNR gains. The results are presented in TABLE I.

Fig. 7(a) illustrates that the proposed MPWI-CCC outperforms CPWC and MPWI-HD in terms of contrast. CR was computed on the anechoic inclusion located at a depth of 40mm from the indicated ROIs in red and blue colors for 2, 4, and 8 plane waves transmission (Fig. 4). In comparison to CPWC, CR gains of 5.80dB, 10.70dB, and 13.50dB were achieved, while only 0.91dB, 4.54dB, and 7.87dB were obtained with MPWI-HD. Fig. 7(b) compares the -6dB axial resolution calculated on scatterer at a depth 35mm and azimuth -10mm. All the imaging schemes exhibit nearly identical

TABLE I: SNR gains obtained with MPWI-CCC with diffrent setups and the gains obtained with MPWI-HD with the same number of transmissions compared to the CPWC reference method.

PWs	Number of bits	MPWI-CCC (dB)	MPWI-HD (dB)
2	4	8.60	2.18
4	4	12.66	6.20
	8	15.43	
	16	17.73	
8	4	15.06	9.72
	8	18.01	
	16	21.39	

axial resolution for the different numbers of plane wave transmissions with a small degradation of 0.02mm for MPWI-CCC. This highlights that the proposed MPWI-CCC does not severely deteriorate the axial resolution which is attributed to the ideal correlation properties of (N, N, NM/P)-CCC.

The simulated power Doppler images are depicted in Fig. 5 for a blood flow in a 2 mm blood vessel with a flow rate of 2 ml/s. The images are presented for three imaging schemes with 2 and 4 angle transmissions. The number of bits in (N, N, MN/P)-CCC sequences was set to 4 bits, and the simulations were conducted under -5dB noise conditions relative to the blood signal. A visual inspection shows that flow perceptibility was enhanced using the proposed MPWI-CCC for both 2 and 4 angle transmissions compared to CPWC and MPWI-HD. The noise level around the vessel decreased for the case of 2 angle transmissions, and it was completely suppressed (w.r.t the dynamic range) in the case of 4 angle transmissions, enabling better power Doppler assessment.

Fig. 8(a) validates these visual assessments by depicting the SNR measurements in the simulated power Doppler images. As expected, CPWC yields the lowest SNR values whatever the number of plane wave, which aligns with the results of Fig. 5. Although both MPWI-HD and MPWI-CCC provide better SNR values, in the case of 2 plane wave transmission, MPWI-HD provides an SNR value of 9.93dB, which is still close to that of CPWC (7.27dB), while MPWI-CCC yields a much higher value of 16.48dB. Fig 8(b) provides a quantitative comparison of the SNR gains achieved by MPWI-HD and MPWI-CCC on the simulated flow phantom. MPWI-HD yields power Doppler SNR gains of 2.65dB, 5.64dB, and 8.81dB while MPWI-CCC yields higher SNR gains with values of 9.20dB, 12.40dB, and 15.50dB for 2, 4, and 8 plane wave transmissions respectively.

Fig. 9(a) shows the normalized axial profiles at azimuth 0mm of the three imaging schemes for 4 plane waves transmission. Compared to the blood signal, the noise level of CPWC is almost at -20dB which reduces the detectability of blood signal. The noise was decreased to around -31 dB for MWPI-HD and an even further decrease to around -45dB was obtained with the proposed MPWI-CCC. These observations were validated by CR values calculated on power Doppler images and depicted in Fig. 9(b). Compared to CPWC, MPWI-HD yields CR gains of 5.27dB, 11.30dB and 17.54dB for 2,4

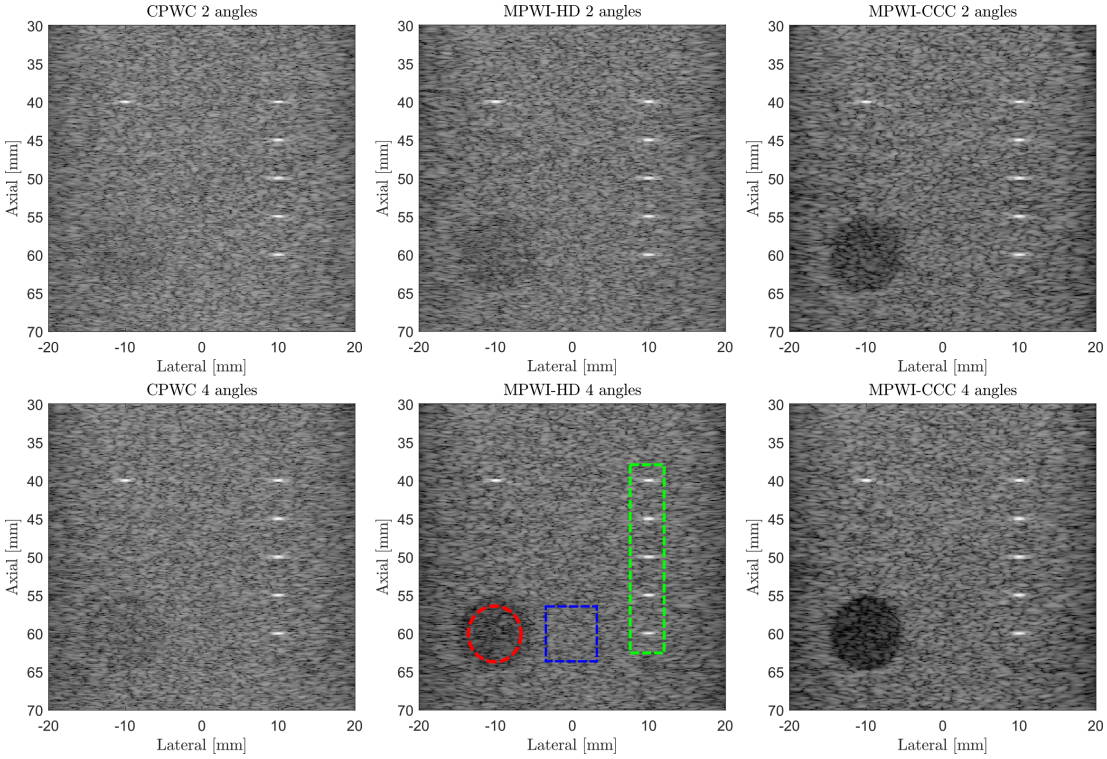

Fig. 4: The simulated B-mode images of the tissue-mimicking phantom for CPWC, MPWI-HD and MPWI-CCC for 2 and 4 plane waves transmissions. Dynamic range is set to -60dB for all images.

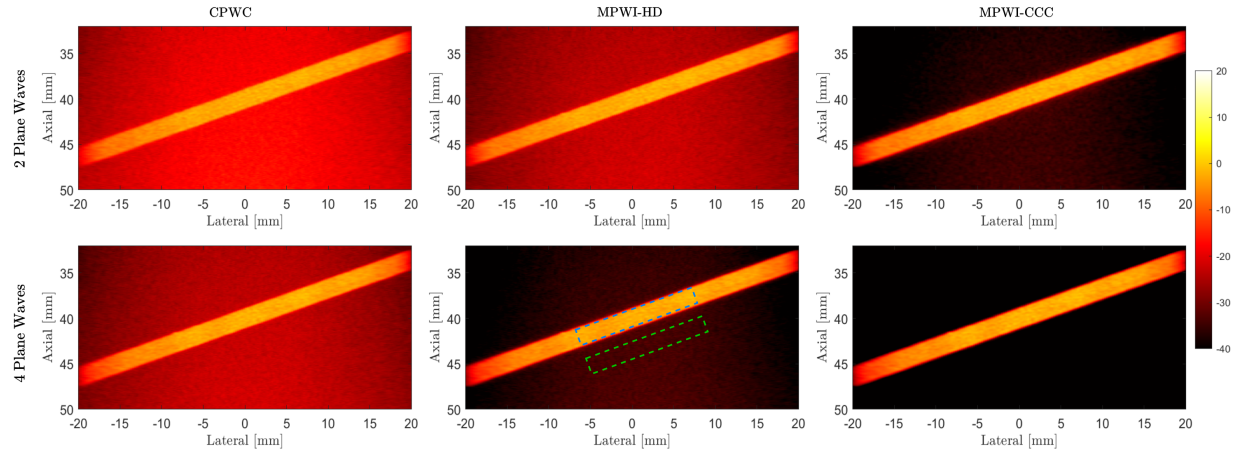

Fig. 5: The simulated power Doppler images for CPWC, MPWI-HD and MPWI-CCC for 2 and 4 plane waves transmissions.

and 8 plane waves transmission while values of 18.04 dB, 24.35dB and 30.16dB are obtained with the proposed MPWI-CCC.

B. Experimental Results

Similar to the simulated PSFs, a wire phantom experiment was conducted in water to mimic a PSF with 4 plane waves transmission. In Fig. 10, a lateral line plot over the wire placed at a depth of approximately 33 mm is shown to evaluate the effect of the encoding methods on the lateral response. The Verasonics transmit voltage was set to 15 V for all three methods to ensure high SNR conditions, which explains the similar noise floor observed across the methods. The results show that at the -6 dB level, the lateral resolution is slightly affected by MPWI-HD and MPWI-CCC, with measured resolutions of 0.46 mm and 0.49 mm, respectively, compared to 0.42 mm for CPWC. However, at lower intensity levels, such as -20 dB, the lateral response degrades more noticeably for MPWI-HD and MPWI-CCC, which yield resolutions of 1.20 mm and 1.30 mm, respectively, while CPWC maintains a finer resolution of 0.70 mm.

The results of the flow experiment conducted using the commercial flow phantom setup are depicted in Fig. 11 for the three imaging schemes (CPWC, MPWI-HD and MPWI-CCC) with 2 and 4 plane wave transmissions. Power Doppler maps are overlayed on B-mode images of the tissue mimicking

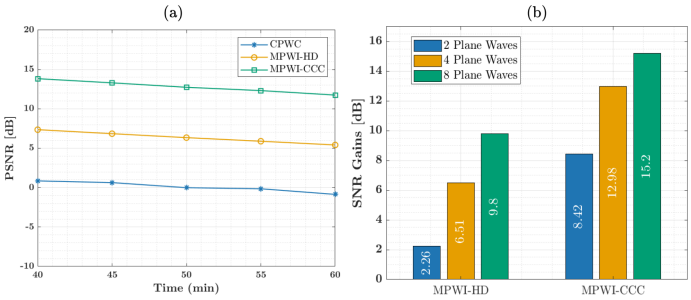

Fig. 6: (a) PSNR values measured on the 5 scatterers indicated in the green box of Fig. 4 using equation 12. (b) SNR gains obtained with MPWI-HD and MPWI-CCC compared to CPWC for 2, 4 and 8 plane waves transmissions for the simulated tissue mimicking phantom.

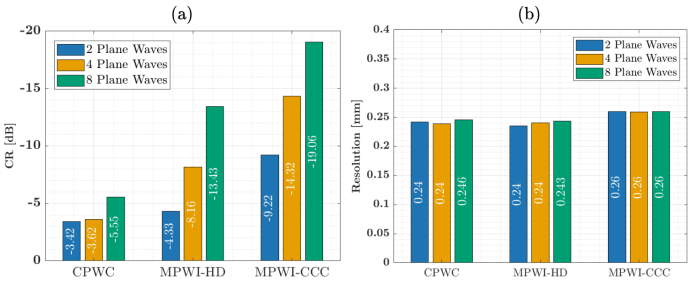

Fig. 7: (a) CR and (b) Axial resolution values for the simulated tissue mimicking phantom.

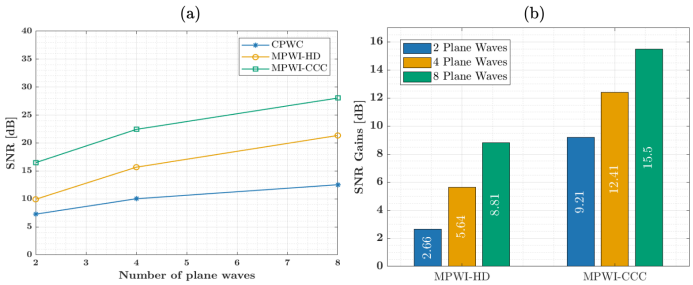

Fig. 8: (a) SNR and (b) SNR Gains computed for the simulated power Doppler images for 2, 4 and 8 plane waves transmissions.

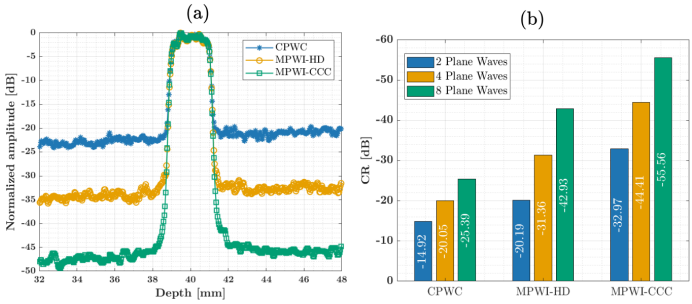

Fig. 9: (a) The normalized axial profiles on the simulated power Doppler images at azimuth 0mm for 4 plane waves transmissions. (b) CR values computed on the simulated power Doppler images in Fig. 6

phantom, shown with a dynamic range of -20dB, to visually compare the Doppler signal and noise levels of CPWC, MPWI-HD, and the proposed MPWI-CCC. To generate the power Doppler maps, 200 frames were acquired and beamformed using DAS, then clutter filtered through an SVD filter. The SVD filter was applied to remove tissue signals, retaining only blood and noise signals in the dataset, which were then summed to form the power Doppler images. It is important to note that the noise was not filtered with SVD to better highlight the effects of MPWI-HD and MPWI-CCC on the noise level of the images.

By qualitatively analysing Fig. 11, we see that MPWI-CCC generates power Doppler images of enhanced quality compared to CPWC and MPWC-HD. In the case of CPWC, the blood signal is barely visible due to the high noise level surrounding the vessel for both 2 and 4 plane waves transmissions. With MPWI-HD, the visibility of the blood flow remains poor when transmitting with 2 plane waves but improves with 4 plane waves. However, the noise level around the vessel remains high. In contrast, power Doppler images obtained with MPWI-CCC exhibit strong blood flow signals with reduced noise levels around the vessel for both 2 and 4 plane wave transmissions.

These visual observations were qualitatively validated by calculating the SNR on the Doppler images using the ROIs in Fig. 11, and the results are depicted in Fig. 12(a). It shows that for 2, 4, and 8 plane waves transmissions, CPWC fails to provide positive SNR, with values of -2.33dB, -2.06dB and -1.86dB respectively. On the other hand, MPWI-HD yields an SNR close to 0dB for 2 plane waves transmission, which aligns with the poor Doppler flow visibility in Fig. 11. However, the SNR values increase to 5dB and 7dB with an increasing number of plane waves to 4 and 8. The proposed MPWI-CCC shows higher SNR values than CPWC and MPWI-HD for all plane wave transmission cases, yielding values of 5.48dB, 10.95dB, and 12.27dB for 2, 4, and 8 plane wave transmissions, respectively. Additionally, Fig. 12(b) illustrates the experimental power Doppler SNR gains obtained with MPWI-HD and MPWI-CCC for 2, 4, and 8 plane wave transmissions. Compared to CPWC, MPWI-HD achieves SNR gains of 3.47dB, 6.99dB, and 8.80dB, respectively. However, MPWI-CCC demonstrates superior SNR gains with 7.82dB, 13.02dB, and 14.15dB, highlighting the superior performance of MPWI-CCC in enhancing the power Doppler signal and overall image quality.

In Fig. 13(a), the normalized axial profile at azimuth 0mm for the three imaging schemes, in the case of 4 plane waves transmission, is depicted. For CPWC, the blood signal level is well below the noise level, especially in deeper regions, making it hard to detect the blood flow. The blood signal is enhanced by MPWI-HD and MPWI-CCC; however, the noise level remains higher with MPWI-HD compared to the proposed MPWI-CCC. As a consequence of the SNR enhancement, the CR was also improved by the proposed MPWI-CCC, as depicted in Fig. 13(b). The CR was calculated on power Doppler images using the ROIs indicated in Fig. 11. MPWI-HD achieved CR gains of 0.83dB, 4.29dB, and 4.91dB with respect to CPWC, while values of 4.97dB, 10.08dB, and 11.07dB were achieved with the proposed MPWI-CCC.

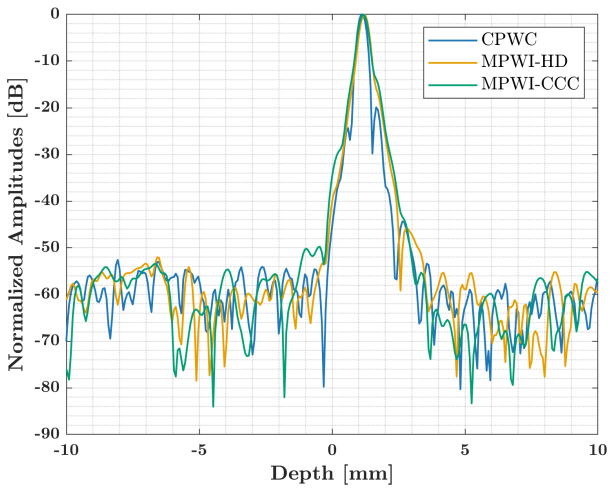

Fig. 10: Lateral line plot over a wire phantom at 33 mm depth providing a sidelobes level comparaison between CPWC, MPWI-HD and MPWI-CCC.

IV. Discussion

In this study, we investigated the performance of a novel coded excitation scheme called Multi-Plane Wave Imaging with Complete Complementary Codes (MPWI-CCC), designed to enhance the SNR in Ultrafast power Doppler imaging. This sequence allows for an increase in SNR by $10\log_{10}(NL)$ compared to CPWC and has been tested in simulation and experimental studies for 2, 4, and 8 plane waves transmissions, along with CPWC and MPWI-HD. This SNR increase translates into better image quality, especially in deep tissue regions where electronic noise is dominant.

To validate the theoretical SNR gains expected with MPWI-HD and MPWI-CCC compared to CPWC, a simulation study was conducted assuming an ideal, linear propagating medium with no frequency-dependent attenuation. Theoretically, an SNR gain of $10\log_{10}(N)$ is expected with MPWI-HD, where N is the number of transmitted plane waves (i.e., transmissions). The simulation results obtained on a tissue-mimicking phantom confirmed this expectation. The measured SNR gains (Fig. 6 (b)) for 2, 4, and 8 plane waves were 2.26dB, 6.51dB, and 9.8dB, respectively, which closely align with the theoretical values of 3.01dB, 6.02dB, and 9.03dB, respectively. The same principle applies to MPWI-CCC, where a theoretical expected gain of $10\log_{10}(NL)$ is anticipated, with N representing the number of plane waves (i.e., transmissions) and L denoting the sequences length. With (N,N,MN/P)-CCC sequences of length 4 bits, the simulation results depicted in Fig. 6(b) illustrate SNR gains of 8.42dB, 12.98dB, and 15.20dB for 2, 4, and 8 plane waves, respectively. These results closely correspond to the theoretical expected gains of 9.03dB, 12.04dB, and 15.05dB, respectively. The same SNR gains observed in the tissue mimicking phantom images are obtained in the simulated power Doppler phantom for both MPWI-HD and MPWI-CCC. This highlights the advantage of MPWI-CCC in providing greater SNR gains compared CPWC than those obtained with MPWI-HD for the same number of transmissions. Furthermore, the results from TABLE I illustrate that MPWI-CCC achieves comparable or even higher SNR with fewer transmissions, resulting in images with high SNR while maintaining a high frame rate compared to MPWI-HD. Additionally, SNR gains can be increased by employing longer sequences while using the same (or fewer) number of transmissions compared to MPWI-HD, leading to a significant enhancement in image quality without sacrificing the frame rate. However, increasing the length of sequences also increases the dead zone area, a point we will discuss later.

For the simulated tissue mimicking phantom and blood flow phantom, noise levels of 5dB and -5dB, were respectively chosen, to mimic real scenarios where the SNR is low, as can occur in deep regions and small vessels with weak blood flow. MPWI-CCC transmits long sequences during each transmission, resulting in more energy delivered to the medium and consequently increasing the SNR of the reconstructed images. The SNR gains obtained with MPWI-CCC allow for an increase in penetration depth compared to CPWC and MPWI-HD. This increase in penetration depth leads to better image contrast, especially in deep regions, enabling better visibility of either the anechoic inclusion or the simulated blood flow (Fig. 7(a) and Fig. 9(b)). Additionally, power Doppler images obtained with MPWI-CCC exhibit stronger blood flow signals and a reduced noise level, enhancing the detectability of blood vessels even with a small number of plane waves (improved frame rate) compared to CPWC and MPWI-HD (Fig. 5). Furthermore, increased penetration depth opens up the possibility of using ultrasound probes with higher central frequencies for improved resolution.

For experimental Doppler imaging on the commercial flow phantom, the system voltage was set to 3 Volts for all three imaging schemes and across all the number of plane wave transmission cases. This low voltage value was chosen to compare the imaging schemes under severe noise conditions and validate the ability of the proposed MPWI-CCC to enhance the Doppler signal in such noisy environments and in low power ultrasound devices such as portable and wearable ultrasound devices. CPWC produced power Doppler images with very poor blood flow signals, even with an increased number of transmitted plane waves, as depicted in Fig. 11. This is attributed to the low transmitted energy and the absence of transmit focusing. The transmitted energy was increased by the quasi-simultaneous transmission of plane waves using either a Hadamard encoding, as in the case of MPWI-HD, or long modulated sequence, as in the case of MPWI-CCC. Even with the low voltage applied to the probe, the images obtained with MPWI-CCC exhibit stronger blood flow signals with reduced noise levels compared to the images obtained with MPWI-HD. This makes MPWI-CCC a valuable tool in applications where low power ultrasound devices are used, such as portable devices.

As discussed earlier, increasing the length of the transmitted sequences increases the SNR gain for the same number of transmitted plane waves. Transmitting long sequences increases the energy transmitted to the medium, improving sensitivity in power Doppler images. However, one of the possible drawbacks of MPWI-CCC is that long sequences may

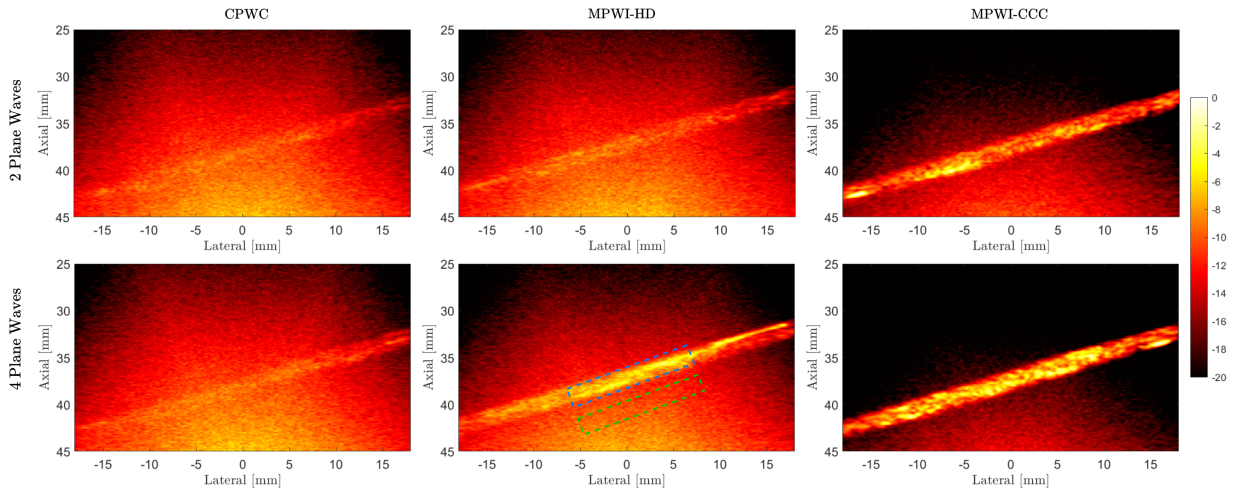

Fig. 11: The experimental power Doppler images on the commercial flow phantom for CPWC, MPWI-HD and MPWI-CCC for 2 and 4 plane waves transmissions.

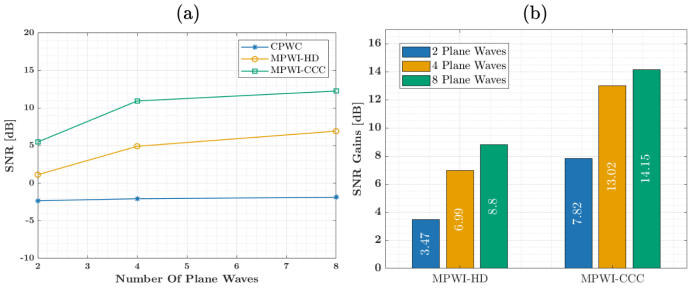

Fig. 12: (a) SNR and (b) SNR gains compared to CPWC computed for the experimental power Doppler images for 2, 4 and 8 plane waves transmissions.

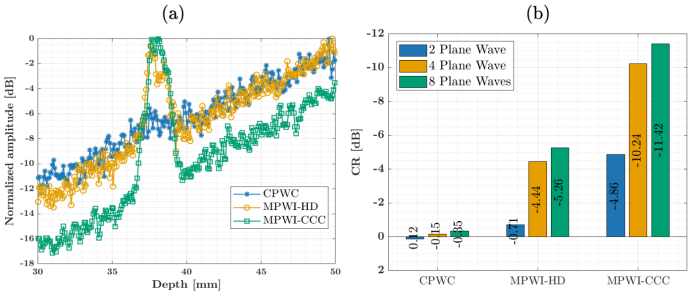

Fig. 13: (a) The normalized axial profiles on the experimental power Doppler images at azimuth 0mm for 4 plane waves transmissions. (b) CR values computed on the images in Fig. 9

expand the dead zone area in the near field since the transducer cannot receive echoes while transmitting. (N,N,NM/P)-CCC sequences, by their nature, enable the reconstruction of short sequences. The size of the dead zone area is proportional to the half of the duration when the transducer is transmitting. In the context of MPWI-CCC, multiple tilted plane waves are transmitted quasi-simultaneously, each separated by a short time delay τ to avoid overlap. Consequently, the dead zone depends on several factors: the number of bits in the sequence transmitted by each plane wave, the duration of the modulated pulse $e(t)$ (in this case, a 1-cycle pulse), the delay τ (equal to the duration of a 1-cycle pulse), and the number of transmitted angles. Another important factor is the delay range across the elements of the array due to the tilt angle of each transmitted wave as illustrated in Fig. 14. Transmitting plane waves at extreme steering angles leads to a broader delay range across the aperture, further extending the overall transmit duration. Taking all these parameters into account and based on the setup used in this study, the total transmit durations for 2, 4, and 8 plane wave transmissions are approximately 2.8μs, 7.5μs, and 22.3μs, respectively. These three cases will give rise to blind zone areas of 2.10mm 5.80mm and 17.2mm respectively. In the cases of 2 and 4 plane waves transmissions, these blind zones remain reasonable especially that it is the deep tissue regions that typically experience low SNR and these regions are in most cases well beyond these blind zone area. However, when sequences with more bits are used alongside a high number of plane waves such as the case of 8 plane waves, consideration should be given to the blind zone area. An approach that will be investigated in the future is the method proposed by [44], [45], where simultaneous plane wave transmission can be employed instead of quasi-simultaneous plane wave transmission. This approach can significantly shorten the transmitted waveform duration, thereby reducing the dead zone area in the near field.

Another possible limitation concerns safety issues associated with the transmission of long sequences. In pulse-echo ultrasound imaging, the Mechanical Index (MI) often serves as a primary constraint, reflecting potential bioeffects such as cavitation due to mechanical disruption, which is proportional to the transmitted waveform voltage [30], [46]. Additionally, the Thermal Index (TI) provides information on potential probe or tissue damage resulting from overheating due to ultrasound absorption [46]. With coded excitation, the SNR gains come from injecting more energy into the medium by increasing the duration of the transmitted waveform. This may raise patient safety concerns and might also cause damage to the probe itself, especially in high-frame-rate scenarios. Care

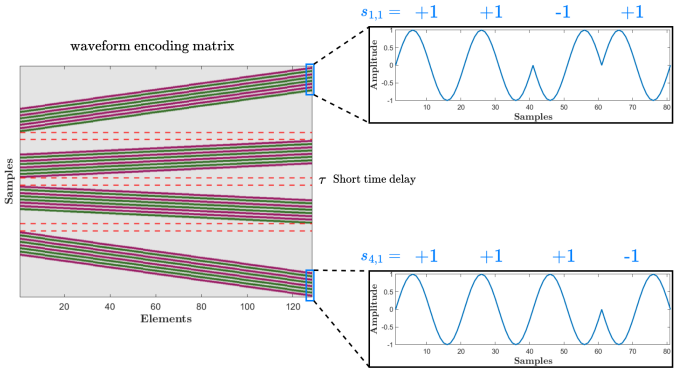

Fig. 14: Schematic representation of the transmit waveforms during a transmission event in MPWI-CCC (4 plane waves). The diagram illustrates the parameters influencing the size of the dead zone area, including the modulated pulse, the number of code bits per plane wave, the delay τ, the number of transmitted angles, and the delay range across the aperture due to steering.

must be taken to ensure that this remains within FDA limits in terms of I_{spta}, MI, and probe temperature. However, in this study, MPWI-CCC is based on the transmission of plane waves, and no focusing is performed. This spreads the energy in the medium, and as a result, the primary constraint to consider is not I_{spta} or MI but the probe temperature. Using plane waves at a high PRF inevitably heats the probe, and the solution is always to reduce the transmit voltage. In this study however, the voltage of the Verasonics was already set to a low value of 3 volts.

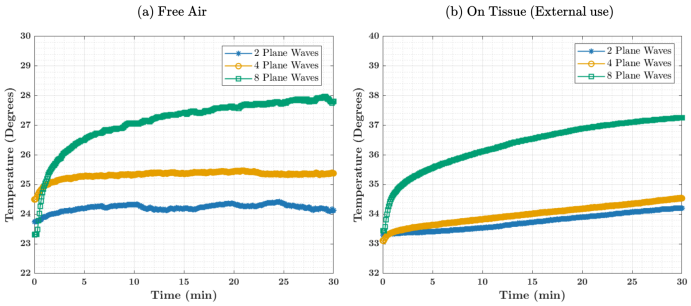

Fig. 15: Temperature curves obtained with MPWI-CCC during 30 minutes measure on (a) Free air (b) On a Tissue-mimicking phantom.

The IEC 60601-2-37 standard specifies safety and performance requirements for ultrasound medical devices, particularly regarding the maximum allowed temperature of the transducer surface [47]. Following this standard, two temperature tests were conducted for the proposed MPWI-CCC using the same experimental setup parameters used for the power Doppler experiments (PRFs, voltage) : testing in a tissue-mimicking phantom and testing in free air. The tissue tests were performed under external-use conditions using the National Physical Laboratory (NPL) temperature test phantom, which is based on agar to mimic the acoustic and thermal properties of human soft tissue. This phantom was designed in accordance with the IEC 60601-2-37 standard. Temperature measurements were conducted using the OpSens AccuSens fiber optic temperature sensor. For the free-air test, the temperature sensor was attached to the surface of the probe.

According to the IEC 60601-2-37 standard, for free-air tests, the initial probe temperature should be $23°C \pm 3°C$ at equilibrium, and the temperature rise should not exceed $27°C$ over a 30 minutes test, with the maximum obtained temperature being $50°C$. For the tissue tests, the temperature of the phantom surface, in contact with the transducer, should not be lower than $33°C$ and must be in thermal equilibrium at the beginning of the test. After 30 minutes of contact, the maximum temperature should not exceed $43°C$, and the temperature rise should not exceed $10°C$.

The temperature test curves obtained with the proposed MPWI-CCC with the transmission of 2, 4, and 8 plane waves in both free-air and tissue tests are shown in Fig. 15. For both tests, the proposed method resulted in maximum temperatures and temperature rises well below the IEC 60601-2-37 standard limits, particularly for 2 and 4 plane waves transmissions. When transmitting 8 plane waves, the test showed a higher temperature rise and maximum temperature, but both remained well below the standard limits, as summarized in Table II.

TABLE II: Comparison the maximum temperature and the temperature rise on free air and on a tissue-mimicking phantom (external use) for MPWI-CCC with 2, 4 and 8 plane waves transmission against the IEC 60601 standards.

Temperature		2 PW	4 PW	8 PW	IEC 60601
Max	**Free Air**	24.43	25.47	28.02	50
	On Tissue	34.22	34.56	37.27	43
Rise	**Free Air**	0.39	0.86	4.70	27
	On tissue	0.92	1.45	3.83	10

It is worth noting that the temperature measurements presented in Fig. 15 were conducted using a low transmit voltage of 3 V, as part of the Doppler experiments performed under severe noise conditions. This setup was designed to emulate challenging clinical scenarios such as imaging deep vessels or patients with thick abdominal walls, significant fat layers where high acoustic attenuation leads to reduced sensitivity to blood flow. Since we did not have access to a physical phantom reproducing these characteristics, the low transmit voltage was used to mimic low-SNR conditions and evaluate the performance of the encoding methods accordingly. In practical scenarios where such attenuation is present, the MPWI-CCC encoding method could indeed be used to increase the transmitted energy beyond the limit of what the scanner can do at peak voltage to further improve the SNR. However, operating at peak voltage with MPWI-CCC would significantly impact the temperature measurements in Fig. 15. In such cases, the experimental parameters must be carefully considered, and the transducer temperature should be closely monitored to avoid excessive heating.

MPWI-CCC leverages the complementary properties of CCC sequences to cancel out correlation sidelobes. However, these approaches require multiple transmissions, making the decoding of plane waves susceptible to motion artifacts. When tissue or blood flow moves between successive transmissions, the correlation sidelobes may not perfectly align in phase. This

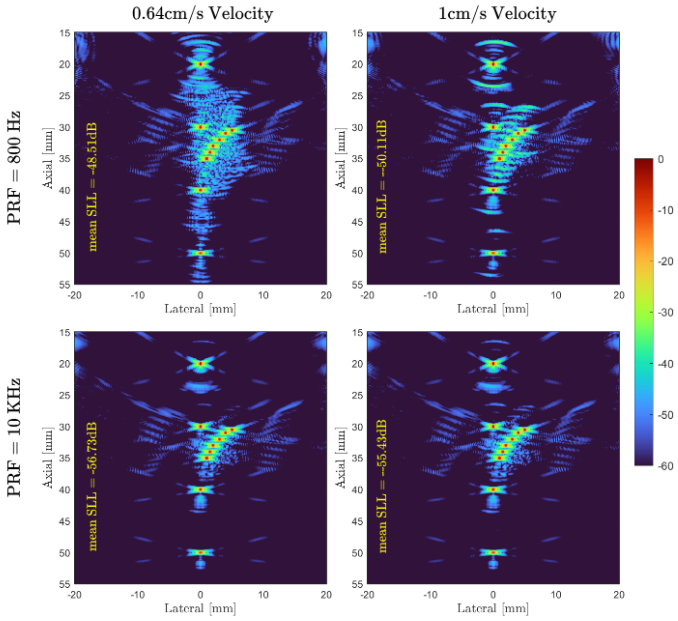

Fig. 16: Simulation of motion related artifacts with two velocities 0.64cm/s and 1cm/s at two PRFs 800Hz and 10KHz

misalignment introduces correlation sidelobes that manifest as artifacts in the image, reducing contrast. For example, in abdominal ultrasound applications, tissue motion due to breathing and cardiac activity can vary from 1 to 5 cm/s. Normal breathing can cause abdominal organs to move at velocities of 1 to 3 cm/s, with heavy breathing reaching up to 5 cm/s. Cardiac motion can induce tissue velocities of up to 1 cm/s. These motion velocities can compromise the effectiveness of the decoding process, especially at lower frame rates. At higher frame rates, motion-induced artifacts remain at an acceptable level, as shown in Fig. 16. Moreover, since only power Doppler imaging is considered, which is not sensitive to flow direction and does not require velocity estimation. This makes it less affected by sidelobe artifacts, as their magnitude is reduced through the clutter filtering step. However, in flow imaging applications where velocity estimation is required, particularly using the phase shift estimator, motion artifacts can lead to incorrect velocity estimations and the appearance of artificial flow regions at very high velocities [48]. In these situation motion artifacts must be addressed. In the literature motion correction has been extensively studied, and some methods have been proposed in order to compensate for this decoding error introduced by motion when complementary binary sequences are used [48], [49]. These techniques can potentially be extended to correct motion artifacts introduced by the MPWI-CCC method. Additionally, various motion correction approaches have been proposed in scenarios where coded excitation is not used, such as in high-frame-rate imaging sequences requiring coherent compounding [50]–[52], synthetic transmit aperture imaging [53]–[57], blood flow imaging [51], [58]–[60], and ultrasound localization microscopy [61], [62]. However, the adaptability of these techniques to coded excitation still needs to be investigated.

Additionally, nonlinearities in acoustic propagation can distort transmitted waveforms, causing deviations from their ideal shapes and spectra. This distortion can compromise the performance of pulse compression techniques by reducing their ability to effectively cancel sidelobes [63]. For instance, harmonic distortions in nonlinear media can degrade peak sidelobe level performance, particularly for binary phase-modulated coded excitation methods [64]. In the case of MPWI-CCC, nonlinear propagation primarily affects the waveform compression and rarefaction phases, altering their velocities and amplitudes. These distortions impact the performance of matched filter decoding, as it relies on a linear model of received signals, leading to suboptimal decoding. However, MPWI-CCC can mitigates some of these effects by taking benefits of frequency-dependent attenuation, as described in [27] for pulse compression methods. Higher-frequency harmonic components are reduced due to frequency-dependent attenuation, thereby preserving the complementary summation to some extent. Additionally, safety limits in medical ultrasound imaging reduces the occurrence of such nonlinear effects [64], and the reduced transmit voltage used in our setup further minimizes nonlinearities in the medium. Thus, while nonlinear propagation imposes certain limitations, our approach remains effective within its intended application scope.

In this study, MPWI-CCC has primarily been applied to ultrafast power Doppler imaging. Other ultrafast plane wave imaging applications suffering from low SNR may also benefit from MPWI-CCC, such as shear wave elastography will be considered in future works.

V. Conclusion

To address the problem of the low SNR of CPWC , which limits the sensitivity of ultrafast power Doppler imaging, we proposed a new imaging sequence named Multi-Plane Wave Imaging with Complete Complementary Codes (MPWI-CCC). Leveraging the ideal correlation properties of (N,N,MN/P)-CCC binary sequences, our method involves quasi-simultaneously transmitting tilted plane waves, each carrying a distinct sequence during every transmission event. The received echoes are decoded as if the plane waves were transmitted individually, but with higher SNR. Furthermore, the nature of (N,N,MN/P)-CCC allows for the generation of shorter sequences, thus preventing the occurrence of large dead zone areas. Through a combination of experimental and simulation studies, we demonstrated that MPWI-CCC outperforms CPWC and MPWI-HD in terms of both SNR and contrast, with a negligible decrease of the axial resolution. The enhanced SNR offered by MPWI-CCC enables more accurate detection of blood flow signals and increased penetration depth, offering potential benefits for various clinical applications. However, it is important to acknowledge potential limitations of this approach, such as the impact of attenuation and motion on decoding accuracy, as well as the potential expansion of the blind zone area when transmitting a large number of plane waves, which will be subject to future investigation.

ACKNOWLEDGMENT

The authors would like to thank the members of the ANR SPARTECHUS Project for the suggestions and feedbacks on our work. A special thanks also to François Varray and Celestine Lachambre for the insightful discussions.

REFERENCES

[1] J. M. Rubin, R. O. Bude, P. L. Carson, R. L. Bree, and R. S. Adler, "Power doppler us: a potentially useful alternative to mean frequency-based color doppler us." *radiology*, vol. 190, no. 3, pp. 853–856, 1994.

[2] J. M. Rubin, R. S. Adler, J. B. Fowlkes, S. Spratt, J. E. Pallister, J.-F. Chen, and P. L. Carson, "Fractional moving blood volume: estimation with power doppler us." *Radiology*, vol. 197, no. 1, pp. 183–190, 1995.

[3] D. Maresca, M. Correia, M. Tanter, B. Ghaleh, and M. Pernot, "Adaptive Spatiotemporal Filtering for Coronary Ultrafast Doppler Angiography," *IEEE Transactions on Ultrasonics, Ferroelectrics, and Frequency Control*, vol. 65, no. 11, pp. 2201–2204, Nov. 2018. [Online]. Available: https://ieeexplore.ieee.org/document/8466597/

[4] B. Pialot, A. Bernard, H. Liebgott, and F. Varray, "Sensitivity Enhancement Using Chirp Transmission for an Ultrasound Arthroscopic Probe," *IEEE Transactions on Ultrasonics, Ferroelectrics, and Frequency Control*, vol. 69, no. 10, pp. 2776–2784, Oct. 2022. [Online]. Available: https://ieeexplore.ieee.org/document/9738618/

[5] E. Macé, G. Montaldo, I. Cohen, M. Baulac, M. Fink, and M. Tanter, "Functional ultrasound imaging of the brain," *Nature Methods*, vol. 8, no. 8, pp. 662–664, Aug. 2011. [Online]. Available: https://www.nature.com/articles/nmeth.1641

[6] E. Mace, G. Montaldo, B.-F. Osmanski, I. Cohen, M. Fink, and M. Tanter, "Functional ultrasound imaging of the brain: theory and basic principles," *IEEE Transactions on Ultrasonics, Ferroelectrics and Frequency Control*, vol. 60, no. 3, pp. 492–506, Mar. 2013. [Online]. Available: http://ieeexplore.ieee.org/document/6470411/

[7] T. Deffieux, C. Demene, M. Pernot, and M. Tanter, "Functional ultrasound neuroimaging: a review of the preclinical and clinical state of the art," *Current Opinion in Neurobiology*, vol. 50, pp. 128–135, Jun. 2018. [Online]. Available: https://linkinghub.elsevier.com/retrieve/pii/S0959438817302465

[8] L. Mo, Ting-Lan Ji, Ching-Hua Chou, D. Napolitano, G. McLaughlin, and D. DeBusschere, "Zone-based color flow imaging," in *IEEE Symposium on Ultrasonics, 2003.* Honolulu, HI, USA: IEEE, 2003, pp. 29–32. [Online]. Available: http://ieeexplore.ieee.org/document/1293350/

[9] J. Bercoff, G. Montaldo, T. Loupas, D. Savery, F. Mézière, M. Fink, and M. Tanter, "Ultrafast compound doppler imaging: providing full blood flow characterization," *IEEE Transactions on Ultrasonics, Ferroelectrics and Frequency Control*, vol. 58, no. 1, pp. 134–147, Jan. 2011. [Online]. Available: http://ieeexplore.ieee.org/document/5688407/

[10] S. I. Nikolov and J. A. Jensen, "Velocity estimation using synthetic aperture imaging [blood flow]," in *2001 IEEE Ultrasonics Symposium. Proceedings. An International Symposium (Cat. No. 01CH37263)*, vol. 2. IEEE, 2001, pp. 1409–1412.

[11] ——, "In-vivo synthetic aperture flow imaging in medical ultrasound," *IEEE transactions on ultrasonics, ferroelectrics, and frequency control*, vol. 50, no. 7, pp. 848–856, 2003.

[12] J. Bercoff, M. Tanter, and M. Fink, "Supersonic shear imaging: a new technique for soft tissue elasticity mapping," *IEEE Transactions on Ultrasonics, Ferroelectrics and Frequency Control*, vol. 51, no. 4, pp. 396–409, Apr. 2004. [Online]. Available: http://ieeexplore.ieee.org/document/1320804/

[13] J. Udesen, F. Gran, K. L. Hansen, J. A. Jensen, C. Thomsen, and M. B. Nielsen, "High frame-rate blood vector velocity imaging using plane waves: Simulations and preliminary experiments," *IEEE transactions on ultrasonics, ferroelectrics, and frequency control*, vol. 55, no. 8, pp. 1729–1743, 2008.

[14] G. Montaldo, M. Tanter, J. Bercoff, N. Benech, and M. Fink, "Coherent plane-wave compounding for very high frame rate ultrasonography and transient elastography," *IEEE Transactions on Ultrasonics, Ferroelectrics and Frequency Control*, vol. 56, no. 3, pp. 489–506, Mar. 2009. [Online]. Available: http://ieeexplore.ieee.org/document/4816058/

[15] M. Tanter and M. Fink, "Ultrafast imaging in biomedical ultrasound," *IEEE Transactions on Ultrasonics, Ferroelectrics, and Frequency Control*, vol. 61, no. 1, pp. 102–119, Jan. 2014. [Online]. Available: https://ieeexplore.ieee.org/document/6689779/

[16] C. Demene, T. Deffieux, M. Pernot, B.-F. Osmanski, V. Biran, J.-L. Gennisson, L.-A. Sieu, A. Bergel, S. Franqui, J.-M. Correas, I. Cohen, O. Baud, and M. Tanter, "Spatiotemporal Clutter Filtering of Ultrafast Ultrasound Data Highly Increases Doppler and fUltrasound Sensitivity," *IEEE Transactions on Medical Imaging*, vol. 34, no. 11, pp. 2271–2285, Nov. 2015. [Online]. Available: http://ieeexplore.ieee.org/document/7098422/

[17] B. Pialot, L. Augeul, L. Petrusca, and F. Varray, "A simplified and accelerated implementation of SVD for filtering ultrafast power Doppler images," *Ultrasonics*, vol. 134, p. 107099, Sep. 2023. [Online]. Available: https://linkinghub.elsevier.com/retrieve/pii/S0041624X23001750

[18] R. Paridar and B. M. Asl, "Frame rate improvement in ultrafast coherent plane wave compounding," *Ultrasonics*, vol. 135, p. 107136, Dec. 2023. [Online]. Available: https://linkinghub.elsevier.com/retrieve/pii/S0041624X23002123

[19] J. A. Jensen, *Estimation of blood velocities using ultrasound: a signal processing approach*. Cambridge University Press, 1996.

[20] E. Tiran, T. Deffieux, M. Correia, D. Maresca, B.-F. Osmanski, L.-A. Sieu, A. Bergel, I. Cohen, M. Pernot, and M. Tanter, "Multiplane wave imaging increases signal-to-noise ratio in ultrafast ultrasound imaging," *Physics in Medicine and Biology*, vol. 60, no. 21, pp. 8549–8566, Nov. 2015. [Online]. Available: https://iopscience.iop.org/article/10.1088/0031-9155/60/21/8549

[21] J. Kang, D. Go, I. Song, and Y. Yoo, "Ultrafast Power Doppler Imaging Using Frame-Multiply-and-Sum-Based Nonlinear Compounding," *IEEE Transactions on Ultrasonics, Ferroelectrics, and Frequency Control*, vol. 68, no. 3, pp. 453–464, Mar. 2021. [Online]. Available: https://ieeexplore.ieee.org/document/9146787/

[22] G. Pinton, J.-F. Aubry, E. Bossy, M. Muller, M. Pernot, and M. Tanter, "Attenuation, scattering, and absorption of ultrasound in the skull bone: Absorption of ultrasound in the skull bone," *Medical Physics*, vol. 39, no. 1, pp. 299–307, Dec. 2011. [Online]. Available: http://doi.wiley.com/10.1118/1.3668316

[23] E. Vienneau, A. Weeks, and B. Byram, "Coded Excitation for Increased Sensitivity in Transcranial Power Doppler Imaging," in *2022 IEEE International Ultrasonics Symposium (IUS)*. Venice, Italy: IEEE, Oct. 2022, pp. 1–4. [Online]. Available: https://ieeexplore.ieee.org/document/9958842/

[24] C. Demené, J. Robin, A. Dizeux, B. Heiles, M. Pernot, M. Tanter, and F. Perren, "Transcranial ultrafast ultrasound localization microscopy of brain vasculature in patients," *Nature Biomedical Engineering*, vol. 5, no. 3, pp. 219–228, Mar. 2021. [Online]. Available: https://www.nature.com/articles/s41551-021-00697-x

[25] C. Errico, B.-F. Osmanski, S. Pezet, O. Couture, Z. Lenkei, and M. Tanter, "Transcranial functional ultrasound imaging of the brain using microbubble-enhanced ultrasensitive Doppler," *NeuroImage*, vol. 124, pp. 752–761, Jan. 2016. [Online]. Available: https://linkinghub.elsevier.com/retrieve/pii/S1053811915008526

[26] J. Chomas, P. Dayton, D. May, and K. Ferrara, "Nondestructive subharmonic imaging," *IEEE transactions on ultrasonics, ferroelectrics, and frequency control*, vol. 49, no. 7, pp. 883–892, 2002.

[27] R. Y. Chiao, "Coded Excitation for Diagnostic Ultrasound: A System Developer's Perspective," vol. 52, no. 2, 2005.

[28] T. X. Misaridis, K. Gammelmark, C. H. Jørgensen, N. Lindberg, A. H. Thomsen, M. H. Pedersen, and J. A. Jensen, "Potential of coded excitation in medical ultrasound imaging," *Ultrasonics*, vol. 38, no. 1-8, pp. 183–189, Mar. 2000. [Online]. Available: https://linkinghub.elsevier.com/retrieve/pii/S0041624X99001304

[29] E. Tiran, J. Ferrier, T. Deffieux, J.-L. Gennisson, S. Pezet, Z. Lenkei, and M. Tanter, "Transcranial Functional Ultrasound Imaging in Freely Moving Awake Mice and Anesthetized Young Rats without Contrast Agent," *Ultrasound in Medicine & Biology*, vol. 43, no. 8, pp. 1679–1689, Aug. 2017. [Online]. Available: https://linkinghub.elsevier.com/retrieve/pii/S0301562917301333

[30] Y. Zhang, Y. Guo, and W.-N. Lee, "Ultrafast Ultrasound Imaging With Cascaded Dual-Polarity Waves," *IEEE Transactions on Medical Imaging*, vol. 37, no. 4, pp. 906–917, Apr. 2018. [Online]. Available: https://ieeexplore.ieee.org/document/8170295/

[31] Y. Zhang, H. Li, and W.-N. Lee, "Imaging Heart Dynamics With Ultrafast Cascaded-Wave Ultrasound," *IEEE Transactions on Ultrasonics, Ferroelectrics, and Frequency Control*, vol. 66, no. 9, pp. 1465–1479, Sep. 2019. [Online]. Available: https://ieeexplore.ieee.org/document/8746191/

[32] J. M. K. De Bakker, C. L. De Korte, and A. E. C. M. Saris, "Cascaded plane wave ultrasound for blood velocity vector imaging in the carotid artery," *IEEE Transactions on Ultrasonics,*

Ferroelectrics, and Frequency Control, pp. 1–1, 2024. [Online]. Available: https://ieeexplore.ieee.org/document/10403857/

[33] T. Misaridis and J. Jensen, "Use of modulated excitation signals in medical ultrasound. Part I: basic concepts and expected benefits," *IEEE Transactions on Ultrasonics, Ferroelectrics and Frequency Control*, vol. 52, no. 2, pp. 177–191, Feb. 2005. [Online]. Available: http://ieeexplore.ieee.org/document/1406545/

[34] F. Gran, J. Udesen, M. Nielsen, and J. Jensen, "Coded ultrasound for blood flow estimation using subband processing," *IEEE Transactions on Ultrasonics, Ferroelectrics and Frequency Control*, vol. 55, no. 10, pp. 2211–2220, Oct. 2008. [Online]. Available: http://ieeexplore.ieee.org/document/4638907/

[35] Chenggao Han and N. Suchiro, "A generation method for constructing (N,N,MN/P) complete complementary sequences," in *SympoTIC '04. Joint 1st Workshop on Mobile Future & Symposium on Trends In Communications (IEEE Cat. No.04EX877)*. Bratislava, Slovakia: IEEE, 2004, pp. 70–73. [Online]. Available: http://ieeexplore.ieee.org/document/1409501/

[36] M. Tamraoui, H. Liebgott, and E. Roux, "Complete Complementary Coded Excitation Scheme for SNR Improvement of 2D Sparse Array Ultrasound Imaging," *IEEE Transactions on Biomedical Engineering*, pp. 1–14, 2023. [Online]. Available: https://ieeexplore.ieee.org/document/10287569/

[37] I. Trots, A. Nowicki, and M. Postema, "Ultrasound Image Improvement by Code Bit Elongation," *IEEE Signal Processing Letters*, vol. 25, no. 3, pp. 437–441, Mar. 2018. [Online]. Available: http://ieeexplore.ieee.org/document/8115266/

[38] J. Jensen and N. Svendsen, "Calculation of pressure fields from arbitrarily shaped, apodized, and excited ultrasound transducers," *IEEE Transactions on Ultrasonics, Ferroelectrics and Frequency Control*, vol. 39, no. 2, pp. 262–267, Mar. 1992. [Online]. Available: http://ieeexplore.ieee.org/document/139123/

[39] J. Jensen, "FIELD: A program for simulating ultrasound systems," *Medical and Biological Engineering and Computing*, vol. 34, pp. 351–352, Jan. 1996.

[40] A. Rodriguez-Molares, J. Avdal, H. Torp, and L. Løvstakken, "Axial lobes in coherent plane-wave compounding," in *2016 IEEE International Ultrasonics Symposium (IUS)*. IEEE, 2016, pp. 1–4.

[41] V. Perrot, M. Polichetti, F. Varray, and D. Garcia, "So you think you can DAS? A viewpoint on delay-and-sum beamforming," *Ultrasonics*, vol. 111, p. 106309, Mar. 2021. [Online]. Available: https://linkinghub.elsevier.com/retrieve/pii/S0041624X20302444

[42] D. Garcia, M. Tamraoui, and F. Varray, "Reply to "Comment on "So you think you can DAS? A viewpoint on delay-and-sum beamforming" - Think twice before f-numbering", published by M.F. Schiffner and G. Schmitz," *Ultrasonics*, vol. 138, p. 107222, Mar. 2024. [Online]. Available: https://linkinghub.elsevier.com/retrieve/pii/S0041624X23002986

[43] M. F. Schiffner and G. Schmitz, "Comment on "So you think you can DAS? A viewpoint on delay-and-sum beamforming" [Ultrasonics 111 (2021) 106309]," *Ultrasonics*, vol. 138, p. 107221, Mar. 2024. [Online]. Available: https://linkinghub.elsevier.com/retrieve/pii/S0041624X23002974

[44] F. Nicolet, D. Bujoreanu, E. Carcreff, H. Liebgott, D. Friboulet, and B. Nicolas, "Simultaneous Coded Plane-Wave Imaging Using an Advanced Ultrasound Forward Model," *Applied Sciences*, vol. 12, no. 24, p. 12809, Dec. 2022. [Online]. Available: https://www.mdpi.com/2076-3417/12/24/12809

[45] D. Bujoreanu, A. Bernard, B. Nicolas, H. Liebgott, and D. Friboulet, "Simultaneous coded plane wave imaging: Implementation on a research echograph."

[46] P. Kaczkowski, "Arbitrary Waveform Generation with the Verasonics Research Ultrasound Platform."

[47] F. A. Duck, "Medical and non-medical protection standards for ultrasound and infrasound," *Progress in biophysics and molecular biology*, vol. 93, no. 1-3, pp. 176–191, 2007.

[48] C.-C. Shen and J.-G. Yu, "Slow-time golay decoding for doppler detection of high-velocity blood flow," in *2013 IEEE International Ultrasonics Symposium (IUS)*. IEEE, 2013, pp. 1488–1491.

[49] C. Cannon, J. Hannah, and S. McLaughlin, "Segmented motion compensation for complementary coded ultrasonic imaging," *IEEE transactions on ultrasonics, ferroelectrics, and frequency control*, vol. 57, no. 5, pp. 1039–1050, 2010.

[50] B. Denarie, T. A. Tangen, I. K. Ekroll, N. Rolim, H. Torp, T. Bjåstad, and L. Lovstakken, "Coherent plane wave compounding for very high frame rate ultrasonography of rapidly moving targets," *IEEE transactions on medical imaging*, vol. 32, no. 7, pp. 1265–1276, 2013.

[51] J. Porée, D. Posada, A. Hodzic, F. Tournoux, G. Cloutier, and D. Garcia, "High-frame-rate echocardiography using coherent compounding with doppler-based motion-compensation," *IEEE transactions on medical imaging*, vol. 35, no. 7, pp. 1647–1657, 2016.

[52] S. Salles, F. Varray, D. Garcia, H. Liebgott, and B. Nicolas, "3-d high frame rate imaging with motion compensation (3-d hfr with moco): an experimental evaluation," *IEEE Open Journal of Ultrasonics, Ferroelectrics, and Frequency Control*, vol. 3, pp. 137–145, 2023.

[53] G. E. Trahey and L. F. Nock, "Synthetic receive aperture imaging with phase correction for motion and for tissue inhomogeneities. ii. effects of and correction for motion," *IEEE transactions on ultrasonics, ferroelectrics, and frequency control*, vol. 39, no. 4, pp. 496–501, 2002.

[54] M. Karaman, H. S. Bilge, and M. O'Donnell, "Adaptive multi-element synthetic aperture imaging with motion and phase aberration correction," *IEEE transactions on ultrasonics, ferroelectrics, and frequency control*, vol. 45, no. 4, pp. 1077–1087, 2002.

[55] K. L. Gammelmark and J. A. Jensen, "Duplex synthetic aperture imaging with tissue motion compensation," in *IEEE Symposium on Ultrasonics, 2003*, vol. 2. IEEE, 2003, pp. 1569–1573.

[56] B. Y. Yiu, I. K. Tsang, and C. Alfred, "A modified synthetic aperture imaging approach with axial motion compensation," in *2008 IEEE Ultrasonics Symposium*. IEEE, 2008, pp. 1254–1257.

[57] K. L. Gammelmark and J. Jensen, "2-d tissue motion compensation of synthetic transmit aperture images," *IEEE Transactions on Ultrasonics, Ferroelectrics, and Frequency Control*, vol. 61, no. 4, pp. 594–610, 2014.

[58] I. K. Ekroll, M. M. Voormolen, O. K.-V. Standal, J. M. Rau, and L. Lovstakken, "Coherent compounding in doppler imaging," *IEEE transactions on ultrasonics, ferroelectrics, and frequency control*, vol. 62, no. 9, pp. 1634–1643, 2015.

[59] L. T. Jørgensen, M. Schou, M. B. Stuart, and J. A. Jensen, "Tensor velocity imaging with motion correction," *IEEE Transactions on Ultrasonics, Ferroelectrics, and Frequency Control*, vol. 68, no. 5, pp. 1676–1686, 2020.

[60] V. Pustovalov, D.-H. Pham, J.-P. Remenieras, and D. Kouamé, "Motion compensation for the estimation of high-resolution blood flow in ultrafast ultrasound imaging," in *Medical Imaging 2022: Ultrasonic Imaging and Tomography*, vol. 12038. SPIE, 2022, pp. 72–78.

[61] S. Harput, K. Christensen-Jeffries, J. Brown, Y. Li, K. J. Williams, A. H. Davies, R. J. Eckersley, C. Dunsby, and M.-X. Tang, "Two-stage motion correction for super-resolution ultrasound imaging in human lower limb," *IEEE transactions on ultrasonics, ferroelectrics, and frequency control*, vol. 65, no. 5, pp. 803–814, 2018.

[62] I. Taghavi, S. B. Andersen, C. A. V. Hoyos, M. B. Nielsen, C. M. Sørensen, and J. A. Jensen, "In vivo motion correction in super-resolution imaging of rat kidneys," *IEEE Transactions on Ultrasonics, Ferroelectrics, and Frequency Control*, vol. 68, no. 10, pp. 3082–3093, 2021.

[63] E. Nicolson, D. Lines, E. Mohseni, and C. N. MacLeod, "Single-bit reception with coded excitation for lightweight advanced ultrasonic imaging systems," *IEEE Transactions on Ultrasonics, Ferroelectrics, and Frequency Control*, 2024.

[64] F. Hamilton, P. Hoskins, G. Corner, and Z. Huang, "Nonlinear harmonic distortion of complementary golay codes," *Ultrasonic imaging*, vol. 45, no. 1, pp. 22–29, 2023.